





Age, composition and spatial distribution of sandy loess in north-eastern Germany (Fläming, Brandenburg)

Fabian Kirsten¹  | Joris Starke¹  | Albrecht Bauriegel² | Robert Müller²  |
Jens Jouaux¹ | Christopher Lüthgens³ | Ralf Sinapius⁴ | Jacob Hardt¹ 

¹Department of Earth Sciences, Freie Universität Berlin, Berlin, Germany

²Landesamt für Bergbau, Geologie und Rohstoffe (LBGR) Brandenburg, Cottbus, Germany

³Institute of Applied Geology, Vienna Laboratory for Luminescence Dating (VLL), University of Natural Resources and Life Sciences Vienna, Vienna, Austria

⁴Büro für Bodenkunde, Voigtsdorf, Germany

Correspondence

Fabian Kirsten, Freie Universität Berlin, Department of Earth Sciences, Malteserstraße 74-100, 12249 Berlin Germany
Email: fabian.kirsten@fu-berlin.de

Abstract

The sandy loess deposits in the lowlands of northern Germany present a valuable sedimentary archive for late Weichselian periglacial geomorphodynamics. While other aeolian sediments from the Late Quaternary, especially loess deposits and sand dunes, have been studied and dated in some detail in the last decades, sandy loess has received less scientific attention with respect to its genesis, composition, age and provenance as well as distribution patterns. In this study, we present detailed results for three sediment sections located on the Fläming ridge in the south of the state of Brandenburg. According to our results from luminescence dating, the sandy loess deposits of this area were deposited during the late MIS 2 (19–14 ka) with a highly variable thickness of at least up to 4 m, followed by a deposition of periglacial coversands shortly thereafter. The sandy loess deposits display a homogeneous geochemical composition and grain size characteristics similar to loess sections in the main loess areas to the west and south. Furthermore, we analysed a large dataset of geological drill data and performed a spatial interpolation of sandy loess distribution in the Western Fläming. Despite the strongly dissected modern landscape of the Fläming ridge which is partly the result of intense Holocene soil erosion processes, general patterns of the original loess distribution could be deduced. Based on these findings, we were able to identify the low-lying areas to the north and north-east of the study area to be the most likely source areas for the sandy loess as a result of katabatic winds originating from the Fennoscandian Ice Shield. Thereby, this study yields important insights regarding aeolian transport and deposition patterns under periglacial conditions in the Central European Lowlands.

KEYWORDS

coversand, grain size distribution, kriging, luminescence dating, MIS 2, periglacial, sandy loess, source areas

1 | INTRODUCTION

Loess deposits are important paleo-environmental archives due to their wide-spread distribution and their good suitability for luminescence dating providing robust chronologies. The parameters that control the formation of loess deposits are complex. In Central Europe, they are linked to the Pleistocene dynamics of the Fennoscandian and the Alpine ice sheets and their corresponding periglacial areas

including the glacio-fluvial systems, which provided favorable source areas for windblown particles (Bullard, 2013). The changing climatic conditions during the Pleistocene glacial stages led to changing wind directions and increased wind speeds (Pinto & Ludwig, 2020; Schaffernicht et al., 2020; Vinnepand et al., 2023). Together with a cold climatic reduced vegetation cover, the conditions were set for intense aeolian dynamics (Bosq et al., 2023). The vast European sand belt (Zeeberg, 1998) and the European loess

This is an open access article under the terms of the [Creative Commons Attribution](https://creativecommons.org/licenses/by/4.0/) License, which permits use, distribution and reproduction in any medium, provided the original work is properly cited.

© 2024 The Authors. *Earth Surface Processes and Landforms* published by John Wiley & Sons Ltd.

belt (Lehmkuhl et al., 2021) are reminiscent of the wide extent of the last glacial aeolian processes.

Several recent (meta-)studies have discussed the current knowledge about the definition, genesis and (global) distribution of loess deposits, highlighting their ongoing significance for reconstructing paleo-environmental conditions (Li et al., 2020; Muhs, 2014; Sprafke & Obreht, 2016; Újvári et al., 2016). For (Central) Europe, inter-regional chronologies of loess deposition have been established (Bosq et al., 2023; Zoeller, 2010) and distribution maps have been put forward (Bertran et al., 2016; Haase et al., 2007; Lehmkuhl et al., 2018, 2021), building on a rapidly growing number of studied loess sections.

The youngest loess deposits in Eastern Central Europe date to the Upper Pleniglacial (MIS 2). Four sections in the German state of Saxony-Anhalt (Figure 2) have been studied in detail and numerically dated so far: For the sediment section of Hecklingen studied by Krauß et al. (2016) and Reinecke (2006), the youngest measured depositional ages are in the range of 19–24 ka and for the Zilly section, the youngest ages are at about 15 ka (Schmidt et al., 2021). In Zeuchfeld, the youngest age dates to about 23 ka (Kreutzer et al., 2014), very similar to ages between 22 and 18 ka reported for the section at Zauschwitz (Lauer et al., 2014). For the sediment sections of Ostrau and Seilitz in Saxony, Late Glacial ages between 31 and 15 ka were reported (Meszner et al., 2013). For loess deposits in south-western Poland, Waroszewski et al. (2021) report ages between 23 and 17 ka for six different sites.

Sandy loess deposits have received considerably less attention, despite their spatial and genetic connection to loess deposits and cover sand areas. Sandy loess can be found in comparatively small patches north of and isolated from the main loess areas in northern central Germany (Figure 1). In northern Germany, sandy loess was originally terminologically differentiated into sandy loess *sensu stricto* applied to facies deposited directly adjacent to the main loess areas, while the term *Flottsand* was applied to the spatially isolated patches to the north of the main loess areas (Altermann & Fiedler, 1972a). The sandy loess deposits *sensu stricto* were interpreted as transitional facies between loess and aeolian (cover) sand deposits owing to a function of wind speed and distance from source area(s) (Neumeister, 1965; Siebertz, 1988). However, due to the genetic similarity between sandy loess and *Flottsand*, the term *Flottsand* was abandoned (in 1963), and the term *Sandlöss* (sandy loess) was applied to all deposits with sand and silt contents >20%, respectively (AG Boden, 2005). Furthermore, many sandy loess deposits within the spatially isolated patches have been found to be characterized by a pronounced layering and an alternation of rather fine-grained, silty layers and more coarse-grained, sandy layers. Consequently, these deposits have been labeled 'banded sandy loess' (*Sandstreifenloess*) (Obst & Kainz, 2020).

Sandy loess deposits in the state of Lower Saxony were studied in detail by Gehrt (1994), Gehrt (2014) and Vierhuff (1967). All these deposits are located at elevations below 200 m a.s.l. and the orientation of their distribution pattern is more or less parallel to the former ice margins. The assumed source areas lie within the glacio-fluvial deposits and the ice-marginal valleys (IMVs) in northern Germany. Vierhuff (1967) proposed changing wind directions as the main reason for the grain size differentiation within the sandy loess: While silty components may have come with north-westerly winds over a

distance of 100–200 km from easily erodible glacio-limnic sands (*Beckensande*), the sandy components would have been transported over much shorter distances with westerly to north-westerly, sometimes also easterly winds. Although sandy loess deposits from Lower Saxony have not been dated by luminescence dating so far, they were stratigraphically assigned to the Late Glacial period and interpreted as analogous deposits to the main loess deposits.

The largest distribution area of sandy loess in eastern Germany is found in the south-western tip of the state of Brandenburg on the Fläming ridge. These deposits were described and studied by a number of authors from 1900 onwards (Altermann & Fiedler, 1978; Cepek, 1959; Dammer, 1941; Fiedler & Altermann, 1964; Maudrei, 1968; Nägler, 1926; Nebe et al., 1962; Von Linstow, 1902). However, systematic studies of the sandy loess on the Fläming ridge with respect to age, distribution patterns and provenance are lacking to date. Furthermore, it is yet unclear how these deposits correlate with deposits from the Central European Loess belt.

Therefore, it is the aim of this study to answer the following research questions:

1. When did the deposition of spatially isolated sandy loess deposits in north-eastern Germany take place?
2. How do these deposits compare to the loess deposits from the main loess areas in Germany (Saxony and Saxony-Anhalt) with respect to age and composition?
3. What is the spatial extent of the sandy loess deposits on the Fläming ridge and how does the spatial distribution pattern relate to the geomorphology of the area and the mechanisms of deposition?
4. What can be inferred with respect to potential source areas of the sandy loess deposits on the Fläming ridge and sandy loess deposits in general?

To answer these questions, we conducted sedimentological and geochronological analyses on three newly established sediment sections (Rab 1–3), reassessed a large amount of different available (geological) map sheets and literature sources, and modeled the spatial extent and thickness of the sandy loess on the basis of roughly 1000 soil archive data points provided by the state geological survey.

2 | STUDY AREA

The Fläming ridge is an ice marginal complex in the south-western part of the modern state of Brandenburg (Germany) (Figure 1). The ridge forms the water divide between the Havel watershed to the north and the Elbe watershed to the south. The area reaches a maximum altitude of 200 m a.s.l. at Hagelberg to the west of the town of Bad Belzig, whereas the so-called Lower Fläming to the south and south-east of the town of Jüterbog reaches altitudes of about 100 m a.s.l. (Figure 2).

The morphological expression of the Fläming area as a huge ridge complex is mostly a result of the Saalian advances of the Fennoscandian Ice Sheet (FIS) and the corresponding processes. Saalian glacio-fluvial material is widespread at the surface and patches of Saalian terminal moraines, which approximately follow a lobate shape, stretch from south-east to north-west. The older Saalian (Drenthe) ice advances transgressed all of the study area, whereas the

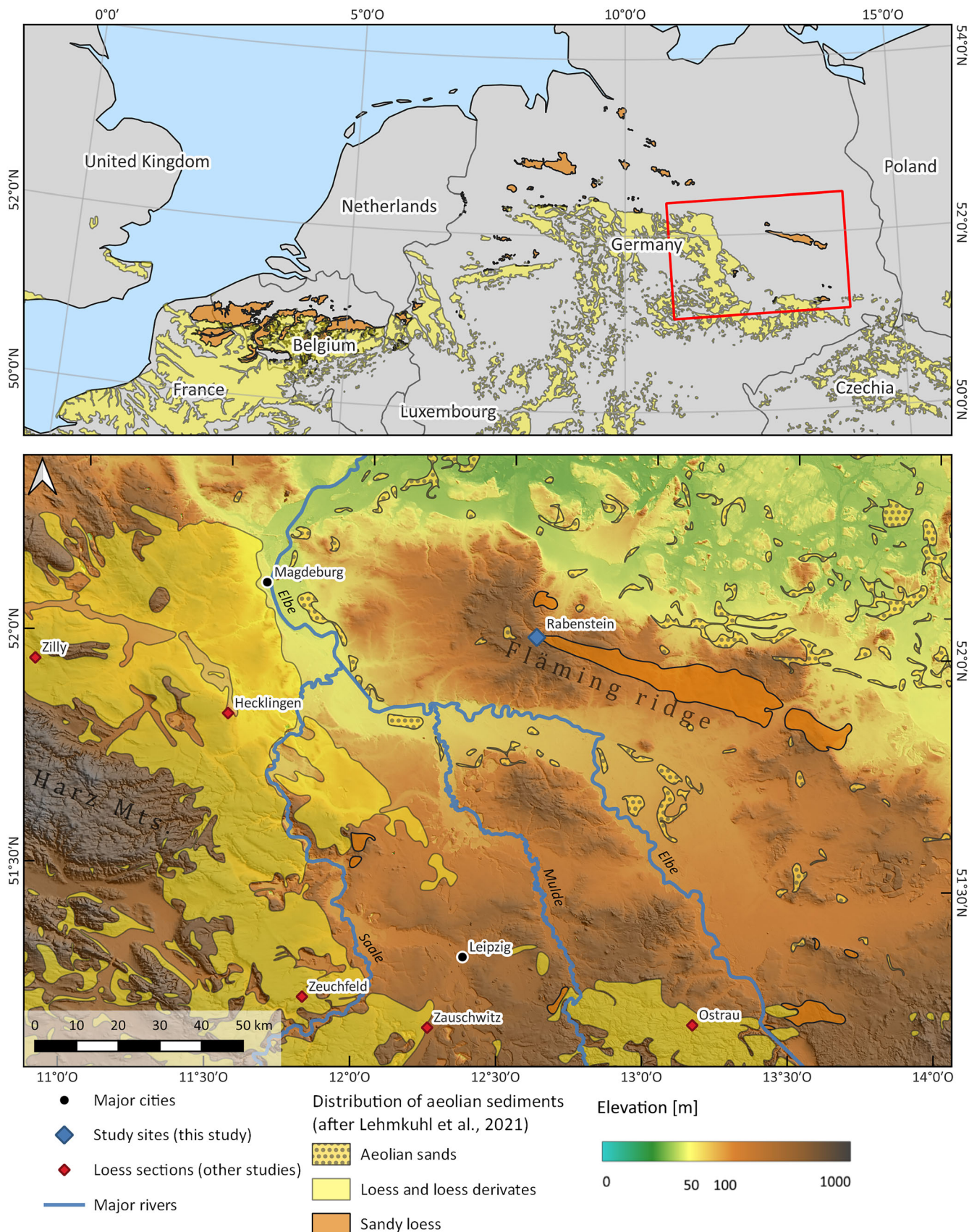


FIGURE 1 (top) Distribution of silty aeolian sediments (loess and sandy loess) in Western and Central Europe [after (Lehmkuhl et al., 2020)]; red rectangle marks the extent of the study area (bottom figure). (bottom) Topography and distribution of aeolian sediments in Eastern-Central Germany. Merged DEM based on (Geobasis-DE/LGB, 2020; GeoSN, 2021; GeoBasisDELVermGeoST), distribution of aeolian sediments based on Lehmkuhl et al. (2020). [Color figure can be viewed at [wileyonlinelibrary.com](https://onlinelibrary.wiley.com)]

younger Saalian (Warthanian) ice advance reached its maximum extent within the study area. Oscillations of the Warthanian ice margin resulted in the accumulation of several tens of metre-thick

packages of glacio-fluvial sand and gravel, partially intercalated with till layers and basin deposits (Eissmann et al., 2020). The oscillating motions of the ice margin with changing directions between north



FIGURE 2 Distribution of sandy loess deposits in the study area [after Lehmkuhl et al. (2020) and LKQ50 (S5)] as well as distribution of Luvisols formed in aeolian sediments (based on the BÜK300 (S5)). Merged DEM based on (Geobasis-DE/LGB, 2020; GeoSN, 2021; GeoBasisDELVermGeoST). The extent of the spatial modelling of sandy loess thickness (Section 3.2) is marked with a black rectangle. [Color figure can be viewed at wileyonlinelibrary.com]

and east are also reflected in the internal deformation structures of the Fläming ridge (Lippstreu et al., 2015). The Warthanian advance corresponds with MIS 6. Correspondingly, north of the Glogau-Baruther IMV (Luckenwalde), OSL ages of near-surface Saalian glacio-fluvial material yielded ages ranging from 150 to 130 ka (Lüthgens et al., 2010).

The Glogau-Baruther IMV lies to the north of the Fläming ridge (Figure 2) and drained the meltwaters of the Weichselian W1 (Brandenburg) advance, which occurred in late MIS 3, as several recent studies have shown based on OSL datings of glacio-fluvial material in Brandenburg (Hardt, 2017; Hardt et al., 2016; Lüthgens et al., 2010, 2020; Lüthgens & Böse, 2011).

In the context of the detailed geological mapping of the Fläming area, the first reports about sandy loess deposits go back to Von Linstow (1902). Observations regarding the properties and distribution of these sediments as well as interpretation regarding their genesis were put forward by a number of authors in the following decades (Altermann, 1993; Altermann & Fiedler, 1978; Cepek, 1959; Dammer, 1941; Fiedler & Altermann, 1964; Maudrei, 1968; Nägler, 1926; Nebe et al., 1962; Von Linstow, 1902).

In the historical geological map sheets 1:25 000 (GK25) of the study area (list of maps given in Table S3), sandy loess deposits are mapped under the term *loesslike dusty sand* ('lössartiger Staubsand'). They were interpreted to be of (late) Weichselian age due to their

stratigraphic position on top of the glacio-fluvial sands and their similarity to loess deposits in the loess areas to the west is stressed (Keilhack, 1906). The sandy loess deposits can be found between 170 m a.s.l. near Garrey in the western part of the study area and 70 m a.s.l. near Dennewitz in the eastern part (Figure 2). Their thickness in the area of Garrey is between 5 and 12 dm, with an increasing thickness towards the west reaching its known maximum of 3.5 m at the very western edge of the sandy loess cover near the castle of Rabenstein (Figure 3). The deposits were found to have a comparatively sharp western and southern boundary marked by pronounced differences in silt contents, while the northern and eastern edge is characterised by a transitional zone between sandy loess and cover sands (*Geschiebedecksand*) (Altermann & Fiedler, 1972a).

On the map, *Lithofazieskarte Quartär* 1:50 000 (LKQ50), the distribution of sandy loess deposits in the study area was subsumed under the term *loess sand* ('Lösssand/Flottsand'). The general distribution of the sandy loess based on all sheets of the LKQ50 covering the study area (S5) corresponds well to the distribution published by Lehmkuhl et al. (2021) based on the Federal Geological Basemap of Germany (1:200 000) (Figure 2).

A special feature of the High Fläming is the so-called 'Rummeln', deeply incised (up to 10 m) V-shaped dry valleys. They are spatially connected to the distribution of sandy loess deposits and follow the outlines of the periglacial dry valleys formed during the Late

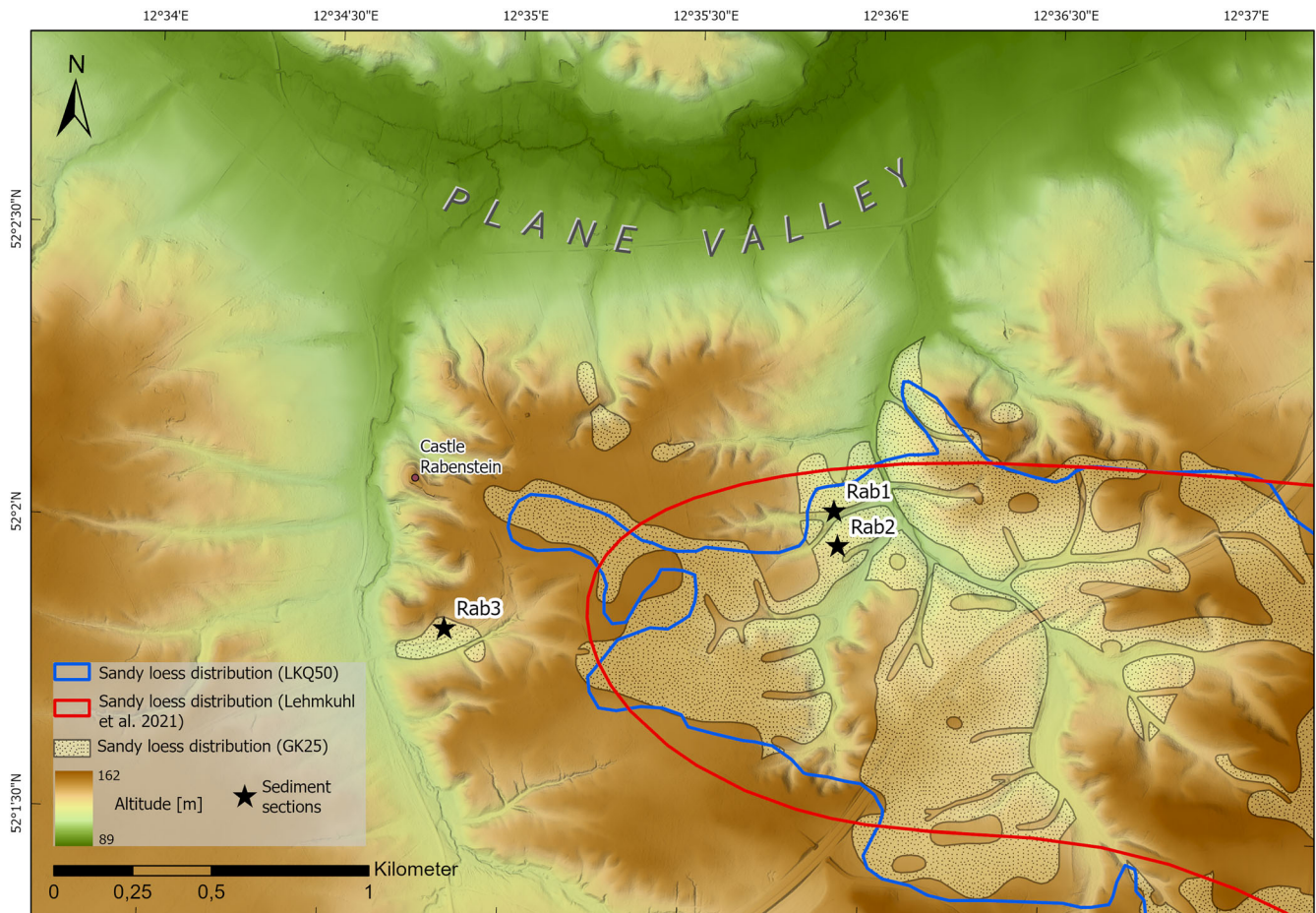


FIGURE 3 Location of sediment sections used in this study before the background of the topography in the study area and the local distribution of sandy loess deposits near Castle Rabenstein [after (Lehmkuhl et al., 2020), LQ50 Brandenburg and GK25 Brandenburg]. [Color figure can be viewed at wileyonlinelibrary.com]

Pleistocene (Liedtke & Marcinek, 2002). Most authors link their current shape to the history of intensified agricultural land use practices since medieval times (Dobers, 2002; Liedtke, 1961; Liedtke & Marcinek, 2002); however, they have not been studied in detail so far. They are very similar to linear erosional features (gullies) known from nearly all intensely used loess areas (Castillo & Gómez, 2016).

In the two adjacent IMVs to the north (Glogau–Baruther IMV) and south (Breslau–Magdeburg–Bremer IMV, current valley of river Elbe) of the Fläming ridge, patchy sandy deposits can be found in the form of dune complexes and sand sheets (*Flugsanddecken*) (Figure 1). These deposits yielded Late Weichselian as well as Late Holocene depositional ages (de Boer, 1995; Hilgers, 2007; Hirsch et al., 2017).

The typical soil type developed in the sandy loess deposits of the Fläming ridge are so-called (*Bänder*)*Fahlerden* in the German soil classification system (AG Boden, 2005), which translates into Retisols or Luvisols in the WRB classification (IUSS Working Group WRB, 2022). Their distribution in the study area (BÜK300, S5) shows a strong spatial correlation to the distribution of sandy loess deposits (Figure 2).

3 | METHODS

3.1 | Sediment sections

At the western edge of the sandy loess area near Rabenstein, three sediment sections were investigated (Figure 3). Their location was

chosen based on field work and soil mappings in the context of the revision of the soil map of the state of Brandenburg. A major factor for site selection was the existence of inorganic carbon in the lower parts of the sections. Increased inorganic carbon contents are considered an indicator of weak pedogenetic alteration of the respective sediments (Kühn et al., 2006).

Section Rab1 (N 52° 2.04732', E 12° 35.90142', 134 m a.s.l.) is located in an upslope position to the north of a periglacial dry valley and was excavated until a total depth of 4.4 m below surface. Section Rab2 (N 52° 1.98768', E 12° 35.91336', 137 m a.s.l.) is located approximately 100 m to the south of Section Rab1 in a plateau position. Section Rab3 (N 52° 1.8246', E 12° 34.82868', 143 m a.s.l.) is located approximately 1 km west of Sections Rab1 and Rab2 near castle Rabenstein, in a mid-slope position at the edge of a small valley head leading southwards into a periglacial dry valley. All three sections are located within forested areas.

From Section Rab1, seven samples were taken for luminescence dating, as well as four undisturbed samples for the preparation of thin sections and subsequent micromorphological analysis. Furthermore, a total number of 32 bulk samples were taken for physical–chemical analysis. In the pedogenetically altered part of the profile (0–170 cm below surface), one sample per soil horizon was taken (a total of seven samples). For the lower part of the profile (170–400 cm below surface), an equidistant sampling strategy was applied in steps of 10 cm each (with a total of 23 samples). Another bulk sample was taken from the layer below 400 cm below surface.

From Section Rab2, four samples were taken for luminescence dating, as well as nine bulk samples for physical–chemical analysis. Sampling depths in this section follow the differentiation into distinct soil horizons established in the field.

From Section Rab3, 10 bulk samples for physicochemical analysis were taken. Like in Section Rab2, sampling depths in this section follow the differentiation into soil horizons established in the field.

The exact sampling depths within the sections can be found in Figure 5, Figure 8 and Figure 10, as well as in S4.

3.2 | Spatial distribution and thickness of sandy loess deposits

We modelled the spatial distribution and thickness of sandy loess deposits by using drill data collected during geologic field campaigns by the Prussian geological survey (Königlich Preußische Geologische Landesanstalt, 1908) at the beginning of the 20th century (Table S5) as well as recent geo-pedological campaigns by the state geological survey of Brandenburg (*Landesamt für Bergbau, Geologie und Rohstoffe LBGR*). The availability of these drill data was restricted to a rectangular area of about 6.5 km × 5 km covering the westernmost part of the main sandy loess area (Figure 2). The drill records ($n = 957$) include information about parent material, enabling us to calculate the thickness of loess deposits at each drill point. Given that the drill depth of these surveys was usually 2 m, records with drill depth above 2 m were truncated in order to avoid drill depth bias.

We then used kriging (Krige, 1951; Matheron, 1963, 1965) to obtain spatial predictions of loess thickness. A linear mixed spatial model composed of a stationary autocorrelated Gaussian random field with isotropic zero-nugget variogram and a trend component was estimated by restricted maximum likelihood (Diggle & Ribeiro Jr., 2007; Patterson & Thompson, 1971; Webster & Oliver, 2007). The trend, modelled as a 0, 1st or 2nd order polynomial in the coordinates, was only included after testing as significant by a Wald-type test (Papritz, 2021; Wald, 1943; Zeileis & Hothorn, 2002). We chose the variogram model as the best fit in terms of log-likelihood. Model performance was assessed by 10-fold cross-validation. To avoid overconfident validation results, we created spatially disjoint data partitions by clustering points based on their coordinates using k -means (Hartigan & Wong, 1979). Geostatistical analysis was conducted using the R software environment (version 4.3.1 R Core Team, 2023) with the R packages *georob* (version 0.3–14 Papritz, 2021), *RandomFields* (Schlather et al., 2022; version 3.3.14 Schlather et al., 2015) and *lmtree* (version 0.9–40 Zeileis & Hothorn, 2002).

3.3 | Laboratory analyses

3.3.1 | Luminescence dating

A total number of 11 samples were taken in light-tight cylinders. Subsequent sample preparation and all luminescence measurements were conducted at the Vienna Laboratory for Luminescence Dating (VLL) under subdued red-light conditions according to standard VLL procedures (Lüthgens et al., 2017; Rades et al., 2018) to obtain potassium-rich feldspar (KFs) grains in the fraction of 150–250 μm . In this study, KFs were

used as a dosimeter for all samples, because no issues related to incomplete bleaching were to be expected because of the (assumed) aeolian nature of the samples, except the lowermost sample VLL-0603-L which was taken from glacio-fluvial sands. Here, bleaching was expected to be an issue, but because of the expected age of the material beyond the last glacial cycle, KFs were also chosen as a dosimeter for this sample in favour of quartz.

Samples were measured at the VLL using small aliquots (1-mm diameter, about 15 grains), except for VLL-0603-L, which was measured using single grains. All measurements were conducted on RISØ TL-OSL DA 20 automated luminescence reader systems (Bøtter-Jensen et al., 2000, 2003, 2010) using IR stimulation (875-nm diodes for single aliquots, 830-nm IR laser for single grains) and detecting the luminescence signal by a photomultiplier through a LOT/Oriel D410/30 optical interference filter, selecting the K-feldspar emission at 410 nm (Krbetschek et al., 1997). A pIRIR225 SAR protocol (post infrared, infrared stimulated single aliquot regenerative dose protocol) (Buylaert et al., 2009; Buylaert et al., 2012) with a stimulation temperature of 225°C and an additional hot bleach step at the end of each SAR cycle to reduce recuperation effects, as determined from dose recovery experiments, was used for all measurements. Details on the experimental setup are available from (Rades et al., 2018) and from the luminescence results table (Table 1).

Radionuclide analyses were conducted at VKTA Rossendorf using high-resolution, low-level gamma spectrometry. All samples were first dried, sealed, and subsequently stored to reach secondary secular Rn equilibrium. All samples were found to be in secular equilibrium and the activities for ^{238}U , ^{232}Th and ^{40}K are presented in the luminescence results table.

Overall dose rates for KFs were found to be rather uniform for all samples, except sample VLL-0603-L, which showed slightly lower values as to be expected. All details on dose rate and age calculation are provided in the luminescence results table (Table 1), which also summarises the ages of the individual samples, as well as average ages (mean \pm standard deviation) for age clusters within each section. The caption of Table 1 provides all necessary information concerning dose rate and age calculation. Results from fading experiments following the approach of Auclair et al. (2003), but were adapted to also include the pIRIR225 signal, revealed low g -values (<1 on average) for the pIRIR225 signal; therefore, fading correction of the ages was not conducted.

3.3.2 | Micromorphological analysis

Thin sections for micromorphological analysis were prepared from oriented and undisturbed soil samples at MKFactory. Analysis of the thin sections was conducted with a polarisation microscope (Bresser Science MPO 401) at magnifications of 25 \times to 400 \times , using plane-polarised (PPL) and cross-polarised light (XPL) and the image analysis software Bresser MicroCamLabII by Susann Heinrich (Leipzig). Microscopic description mainly followed the terminology after Bullock et al. (1985) and Stoops (2003).

3.3.3 | Bulk sample preparation

All bulk samples were air-dried and sieved. The content of coarse fragments >2 mm was discarded, and fine earth (<2 mm) was stored for further analysis. All subsequent analyses were carried out at the Laboratory of the Physical Geography Group in the Department of Earth

TABLE 1 Luminescence results.

Sample lab code	Sample field code	²³⁸ U (Bq/kg)	²³² Th (Bq/kg)	⁴⁰ K (Bq/kg)	Overall dose rate Fs (Gy/ka) ^a	pIRIR225 (n) ^b	pIRIR225 D _e ** (Gy)** ^c	pIRIR225 age (ka) ^d	pIRIR225 average ages (mean ± SD)
VLL-0603-L	RAB1 OSL1	5.39 ± 1.5	4.39 ± 0.35	153.66 ± 13.51	1.24 ± 0.10	7	482.16 ± 28.46	<388 ± 39	n/a
VLL-0603-L SG	RAB1 OSL1	5.39 ± 1.5	4.39 ± 0.35	153.66 ± 13.51	1.24 ± 0.10	144	191.72 ± 12.42	154 ± 16	
VLL-0604-L	RAB1 OSL2	18.79 ± 3.29	23.34 ± 1.54	413.04 ± 26.35	2.52 ± 0.22	20	43.35 ± 1.98	17.2 ± 1.7	17.5 ± 0.7
VLL-0605-L	RAB1 OSL3	19.84 ± 2.76	21.68 ± 1.44	414.27 ± 42.46	2.52 ± 0.24	20	41.50 ± 0.97	16.5 ± 1.7	
VLL-0606-L	RAB1 OSL4	27.40 ± 3.27	27.48 ± 1.79	454.74 ± 37.78	2.86 ± 0.27	18	51.36 ± 3.28	18.0 ± 2.0	
VLL-0607-L	RAB1 OSL5	25.13 ± 4.13	24.74 ± 1.64	461.89 ± 29.44	2.80 ± 0.25	18	50.80 ± 1.13	18.1 ± 1.7	
VLL-0608-L	RAB1 OSL6	29.02 ± 3.66	32.76 ± 2.06	558.17 ± 56.18	3.26 ± 0.32	18	45.51 ± 1.40	14.0 ± 1.4	14.7 ± 0.7
VLL-0609-L	RAB1 OSL7	29.25 ± 3.34	32.57 ± 2.09	556.17 ± 56.55	3.27 ± 0.32	20	50.08 ± 1.17	15.3 ± 1.5	
VLL-0610-L	RAB2 OSL8	24.58 ± 3.03	23.96 ± 1.55	452.47 ± 37.38	2.78 ± 0.25	20	39.61 ± 0.69	14.3 ± 1.3	15.3 ± 1.0
VLL-0611-L	RAB2 OSL9	22.71 ± 2.95	25.78 ± 1.67	465.06 ± 28.80	2.79 ± 0.23	20	45.01 ± 0.92	16.2 ± 1.4	
VLL-0641-L	RAB2 OSL10	11.90 ± 1.55	11.07 ± 0.62	304.01 ± 22.80	2.10 ± 0.17	23	26.41 ± 0.79	12.6 ± 1.1	13.0 ± 0.4
VLL-0642-L	RAB2 OSL11	15.90 ± 1.75	16.33 ± 0.87	336.91 ± 24.93	2.34 ± 0.19	21	31.18 ± 0.91	13.3 ± 1.1	

^aCosmic dose rate determined according to Prescott and Hutton (1994) and Prescott and Hutton (1994), taking the geographical position of the sampling spot (longitude, latitude and altitude), the depth below surface and the average density of the sediment overburden into account. An uncertainty of 10% was assigned to the calculated cosmic dose rate. External and internal dose rates were calculated using the conversion factors of Adamiec and Aitken (1998) and the β -attenuation factors of MEJDAHL (1979), including an alpha attenuation factor of 0.08 ± 0.02 and an internal K content of 12.5 ± 0.5% (Huntley & Baril, 1997) and estimated average water content of 15 ± 5% (all sample but VLL-0603-L) and 10 ± 5% (VLL-0603-L), respectively, throughout burial time. An error was propagated to the overall dose-rate calculation.

^bNumber of aliquots passing all rejection criteria. For sample VLL-0603-L SG number of all single grains passing all rejection criteria.

^cCalculated using the CAM (Galbraith et al., 1999) for all single aliquot samples apart from VLL-0606-L, which showed signs of incomplete bleaching (overdispersion of 16.8 ± 2.8% compared to an average overdispersion of ~10% for the well-bleached samples), thus a MAM-3 (Galbraith et al., 1999) approach; 10% as an overdispersion threshold was used for this sample. For the single grain sample VLL-0603-L SG, the bootstrapped MAM-3 (Cunningham & Wallinga, 2012) using an overdispersion threshold of 20 ± 10% was used for equivalent dose calculation.

^dCalculated using the software ADELE (Kullig, 2005).

Sciences at Freie Universität Berlin [grain size distribution (GSD), magn. susceptibility and colour] and at the state laboratory (Landeslabor) Berlin/Brandenburg (geochemistry, inorganic carbon and pH values).

3.3.4 | Grain size analysis

Two grammes of fine-earth samples (<2 mm) were dispersed using a 10-mL 0.4-N sodium pyrophosphate solution ($\text{Na}_4\text{P}_2\text{O}_7$). Due to the generally low contents of organic matter in our samples (except for the uppermost topsoil samples), removal thereof by treatment with hydrogen peroxide solution (H_2O_2) was omitted. Measurements were performed with a laser diffraction particle size analyser (LS13320, Beckman Coulter with additional PIDS technology) calculating the percentage size frequency within a range of 0.04–2000 μm in 116 discrete grain size classes (Deutsches Institut für Normung, 2020). For the calculation of the grain size distribution (GSD) from the detected light scattering matrix, the MIE-theory was applied (Fluid RI: 1.33, Sample RI: 1.55, Imaginary RI: 0.1), which has been proven to be preferable for loess-paleosol sequences as it reduces/minimises the systematic underestimation of the clay fraction compared to the Fraunhofer estimation (Deutsches Institut für Normung, 2020; Özer et al., 2010; Schulte & Lehmkühl, 2018).

Limits of grain size fractions in this study follow the German soil classification as well as WRB nomenclature (IUSS Working Group WRB, 2022) with the following intervals: fC = 0.04–0.2 μm , mC = 0.2–0.63 μm , cC = 0.63–2 μm , fSi = 2–6.3 μm , mSi = 6.3–20 μm , cSi = 20–63 μm , fS = 63–200 μm , mS = 200–630 μm and cS = 630–2000 μm .

3.3.5 | Geochemical analysis

Element composition analyses were carried out by X-ray fluorescence analysis (XRF) on a PANalytical Zetium 2.4 kW spectrometer (Almelo, Netherlands). The loss on ignition (LOI) was determined by heating 1000 mg of the sample to 105°C (16 h), 550°C (4 h) and 1000°C (2 h), respectively. Heated samples were mixed with the flux lithium metaborate or a mixture of lithium metaborate and lithium tetraborate (for samples with LOI > 25% g/g) and melted into glass beads at 1050°C for 480 s and 1200°C for 25 s. The beads were analysed by wavelength-dispersive XRF.

Hierarchical cluster analysis was implemented using Manhattan distances and Ward's method (Strauss & von Maltitz, 2017). For this purpose, the following geochemical parameters were used: LOI, SiO_2 , TiO_2 , AlO_3 , Fe_2O_3 , MnO , CaO , Na_2O , K_2O , Ba, Cr, Rb, Sr, V, Zn and Zr. In order to address the compositional nature of XRF data and its constant-sum constraint, a compositional data approach was applied (Aitchison, 1982), and all observations were centred log-ratio (clr) transformed. The number of clusters was determined by combining the Dunn index (Dunn, 1974), the silhouette index (Rousseeuw, 1987) and the Jaccard index (Hennig, 2007).

3.3.6 | Inorganic carbon

Calcium carbonate equivalent content was determined using the calcimetry method described by Klosa (1994) (calcimeter

from Feske GmbH). Total inorganic carbon (TIC) was calculated based on the carbonate content in the measured calcium carbonate equivalent.

3.3.7 | pH values

pH values were measured in a 0.0125 mol/L CaCl_2 solution following Deutsches Institut für Normung (2022).

3.3.8 | Magnetic susceptibility

Magnetic properties were analysed using 12 cm^3 of ground subsamples densely packed in rectangular plastic boxes. Volume-specific magnetic susceptibility (κ) was measured at low (0.465 kHz, κLF) and high (4.65 kHz, κHF) frequencies using a Bartington MS3 magnetic susceptibility meter equipped with an MS2B dual frequency sensor. Mass-specific magnetic susceptibility (χ) ($10^{-8} \text{ m}^3/\text{kg}$) was obtained by relating κLF to the mass of each sample.

3.3.9 | Soil colours

Soil colours were determined in dry conditions on the ground sample by measurement of the reflectance between 360 and 740 nm with a photospectrometer (Minolta CM-2500d). Calculation of Munsell colours (D65) was performed based on the spectral data with the software SpectraMagic™ NX Pro Ver. 2.80 by KonicaMinolta.

4 | RESULTS

The following results are mainly discussed within the context of the respective sediment sections. However, for reasons of coherence, we present the detailed results of luminescence dating first before putting them into the context of the individual sediment sections.

4.1 | Spatial distribution of sandy loess deposits

Only 33% of all drill records contain sandy loess layers, resulting in a heavily right-skewed distribution of loess thickness per drill point. Including a 1st order trend in our spatial model reduced the skewness considerably and resulted in a close-to-normal distribution of the residuals. The first-order trend tested as significant, while higher order trends did not. Thus, our final spatial model of sandy loess thickness contained a 1st order trend and an exponential variogram with a range of 84 m and a sill of 3572 cm^2 . Ten-fold cross-validation gave a residual mean squared error of 60 cm.

The kriging predictions of the loess distribution show a clear pattern in the west–east and north–south directions. In the westernmost part of the analysed area, only a few loess patches related to single drilling points exist in a roughly 1.5-km-wide N–S corridor (Figure 4). There are several deep dry valleys, which could have suggested a

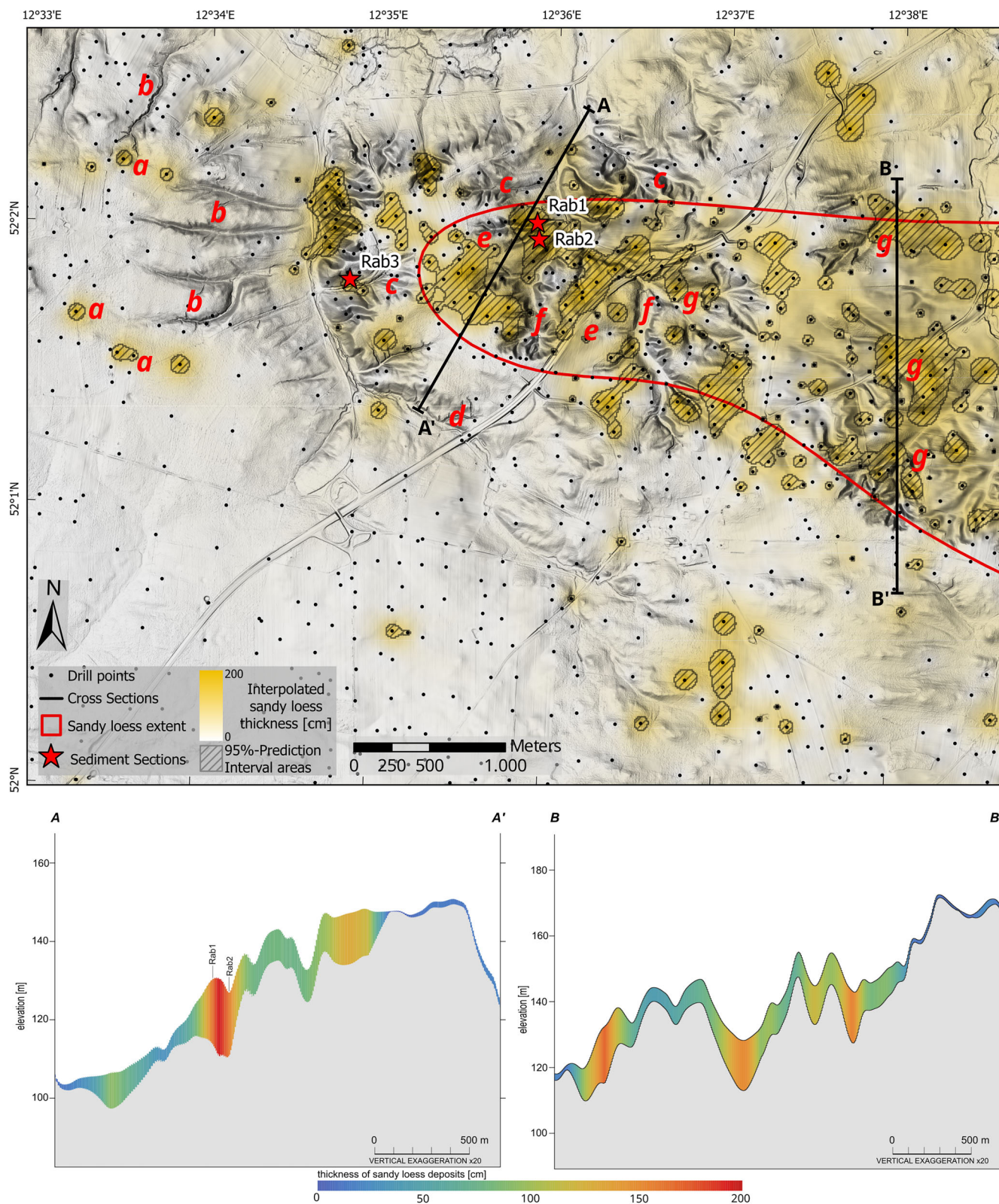


FIGURE 4 Map of kriging predictions of sandy loess thickness in the study area, ranging from 0 cm (white) to 200 cm (yellow) (main figure). Hashed areas indicate regions with an occurrence of loess deposits within the 0.95 kriging prediction interval. Black dots and red stars mark the locations of drill points and sediment sections, respectively. Lowercase letters (red) indicate areas of special interest for geomorphological interpretation discussed in the text (Section 4.1). Sandy loess extent (red outline) is displayed based on data published by (Lehmkuhl et al., 2020, 2021). The background map is a vertically exaggerated hillshade derived from the laser scan digital elevation model (EPSG: 25833). The lower part of the figure: modelled thickness of sandy loess cover (≤ 200 cm) in transects A to A' and B to B', locations marked in the main figure. [Color figure can be viewed at wileyonlinelibrary.com]

more widespread occurrence of loess in this part of the study area. These dry valleys, however, differ in their morphometry from the dry valleys in the main loess areas, as they are more linear and less

internally dissected (Figure 4). The main (sandy) loess accumulation area abruptly starts close to the studied Section Rab3. This onset is accompanied by a clear change in surface morphology: The area is

intensely dissected by dry valleys with dendritic outlines (Figure 4). Outside this modelled accumulation zone, roughly 1 km to the south, the valleys resemble the ones in the westernmost part (Figure 4). Farther to the east, the loess patches become larger and more

continuous, covering the plateau areas of this part of the Fläming ridge (Figure 4). This trend continues eastwards, accompanied by an overall larger north-south extent of the loess cover. In some places, it can be seen that the loess is absent inside the dry valleys (Figure 4).

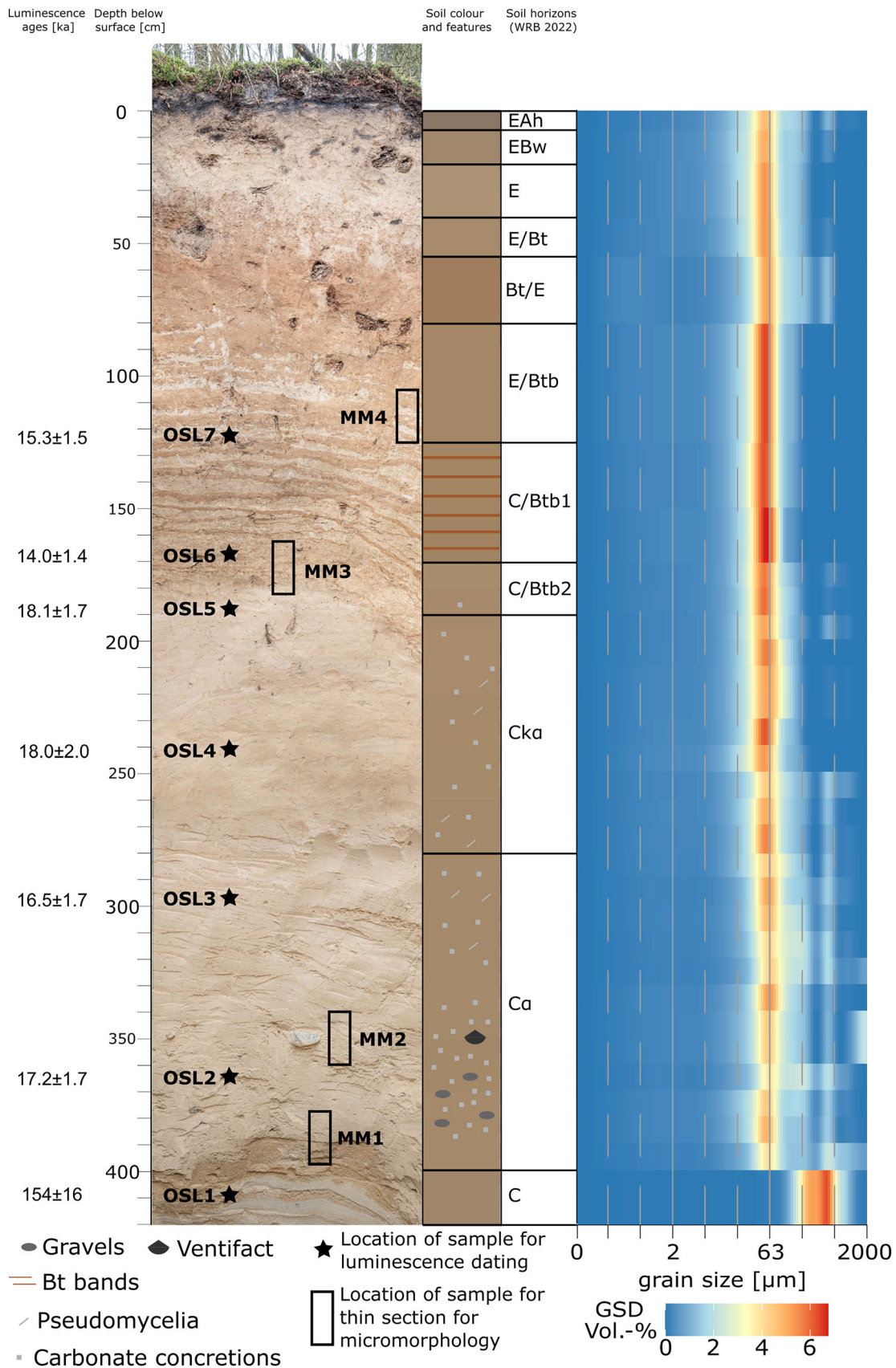


FIGURE 5 Section Rab1: image, sampling locations/depts, soil horizons [IUSS working group WRB 2022], luminescence ages and heat map of grain size distribution. [Color figure can be viewed at wileyonlinelibrary.com]

However, the interpolation in some places also predicts loess deposits inside the dry valleys (Figure 4).

The north–south trend of the loess accumulation is illustrated by both cross-sections: Cross section A–A' with a length of about 2-km cuts through the westernmost tip of the sandy loess area near sediment Sections Rab1 and Rab2 (inset); cross-section B–B' with a length of about 3 km traverses the sand loess area some kilometres further east. Both cross-sections indicate that sandy loess deposits thicker than 100 cm are mainly located on the northern and north-eastern hillslopes of the Fläming ridge, whereas deposits on the highest part of the ridge and on the southern-facing hillslopes are rare and, if they occur, shallow.

4.2 | Luminescence dating

Based on rejection criteria derived from dose recovery experiments (5% recycling, recuperation and test dose error for single aliquots, 20% recycling, recuperation and test dose error for single grains), equivalent doses for all single aliquots show narrow, normally distributed equivalent dose (D_e) distributions and mean equivalent doses were calculated using the central age model (CAM) (Galbraith et al., 1999) as implemented in the R-Luminescence package (Kreutzer et al., 2012). Although single aliquot data for sample VLL-0603-L showed D_e values approaching field saturation in the first tests, the single grain dataset shows a majority of D_e values below $2D_0$ (86% saturation according to [Wintle & Murray, 2006]) and results in a right-skewed distribution with high overdispersion ($50 \pm 3\%$ as determined from CAM calculations), which indicates incomplete bleaching of the luminescence signal prior to deposition. To address this, a bootstrapped version of the three-parameter minimum age model (Cunningham & Wallinga, 2012; Galbraith et al., 1999) with a threshold value of 0.2 ± 0.1 for σ_b was used for the

calculation of a mean D_e . All D_e calculations were conducted using the R-luminescence package (Kreutzer et al., 2012) and are summarised in the luminescence results table (Table 1). Dose–response curves and decay curves for pIRIR225 signals for all samples can be found in Figure S2.

4.3 | Section Rab1

Sediment Section Rab1 (Figure 5) is the reference section of this study, as it was studied in most detail.

The lowest part of the section (>400 cm below surface) is formed by layered sands with a distinct mode in the medium sand fraction (Figure 5). The sands were dated to 154 ± 16 ka (MIS 6).

On top of these sands and separated by a rather sharp boundary, the remaining part of the section (<400 cm below surface) is composed of silty(–sandy) material. This unit displays a rather homogeneous GSD with a distinct mode in the coarse silt fraction between 50 and 60 μm , which is more dominant in the upper part of the unit (Figure 5) (S1). In the lower part, between 250 and 400 cm below surface, a small secondary mode in the medium sand fraction at about 450–500 μm was detected as well as a higher amount of grains in the fine sand fraction (S3). Several horizons/sampling layers in the upper part of the unit display the same mode in the medium sand fraction. This mode can be related to fine layers of (medium) sand in between the mainly silty deposits that were detected macroscopically in the field. These sandy layers are even more abundant in Sections Rab2 (Section 4.4) and Rab3 (Section 4.5).

A considerable amount of coarse fragments including ventifacts is present between 350 and 400 cm below surface. They do not form a continuous stoneline, however. While the lower part of the unit (below 190 cm) contains primary and secondary carbonates (including carbonatic concretions/nodules) and displays a pH between 7.7 and

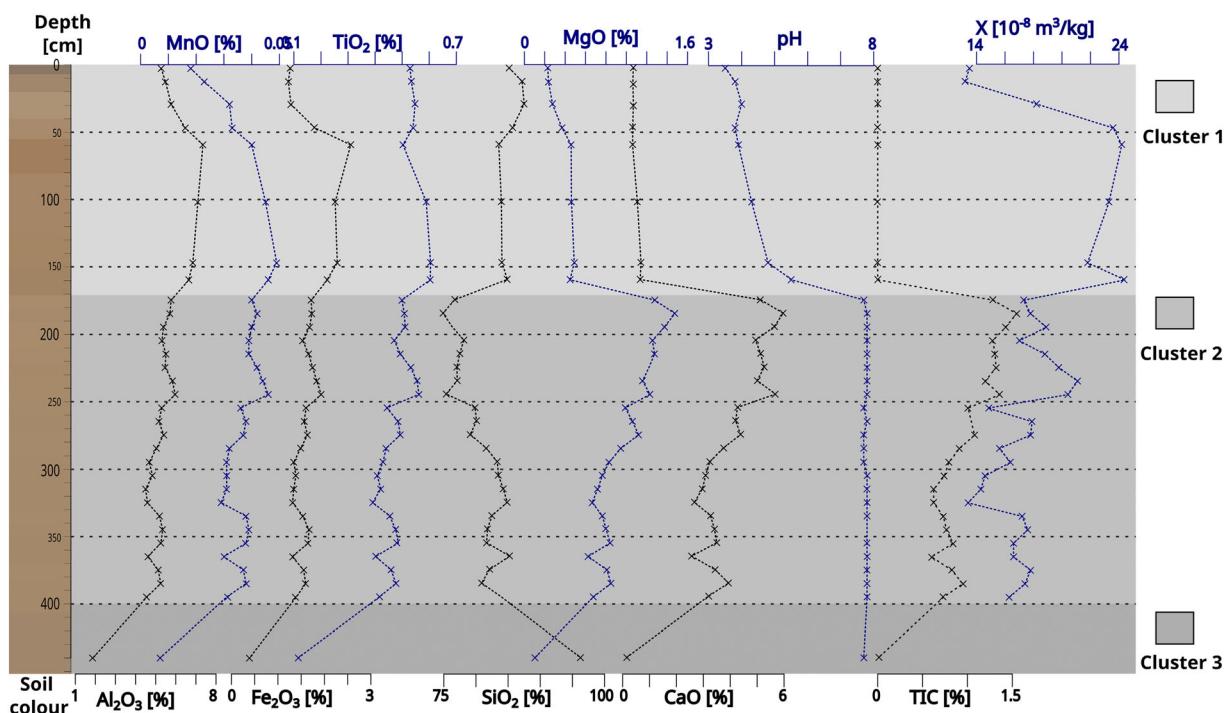


FIGURE 6 Geochemical data and clusters for Section Rab1. [Color figure can be viewed at wileyonlinelibrary.com]

7.8 (Figure 6), the upper (pedogenically altered) part of the section does not contain any carbonates and displays lower pH values between 3.5 (topsoil) and 5. While clay contents in the lower part of the profile are below 5%, they reach a maximum in the Bt horizon at approximately 8% (S3).

With respect to geochemical composition, the upper unit (sandy loess) is mainly composed of SiO_2 (75%–80%), with minor contents of Al_2O_3 (4%–6%) and Fe_2O_3 (1%–2%) (S4). In the pedogenetically altered part of the section (Bt horizons), Al_2O_3 contents reach up to 7.5% and Fe_2O_3 contents up to 2.5%. The geochemical composition is fairly homogeneous, except for contents of CaO, which reach up to 6% at a depth of approximately 2 m. CaO contents in the lower part of the sandy loess (300–400 cm below surface) display values between 2.5% and 3.5%. All samples from the upper part of the section (down to 1.7 m below surface) were assigned to

Geochemical Cluster 1, the lower part to Geochemical Cluster 2. The lowermost (sandy) sample was assigned to the Geochemical Cluster 3.

Luminescence ages for the lower part of the sandy loess deposit (OSL2, OSL3, OSL 4 and OSL5) indicate a mean deposition age of 17.5 ± 0.7 ka (Figure 5; Table 1). Luminescence ages from the upper part of the unit (OSL6 and OSL7) indicate a mean age of 14.7 ± 0.7 ka.

Micromorphological analysis of thin sections from the lower part of the sandy loess deposit (MM1 and MM2) confirmed the macroscopically detected presence of secondary sparitic (in pore spaces) and micritic carbonates (Figure 7e–f). Furthermore, a lenticular platy microstructure (a, b) as well as micritic carbonatic capping of larger grains (c, d) are present. No layering, lamination, crusts or orientations could be detected that would indicate a specific depositional environment.

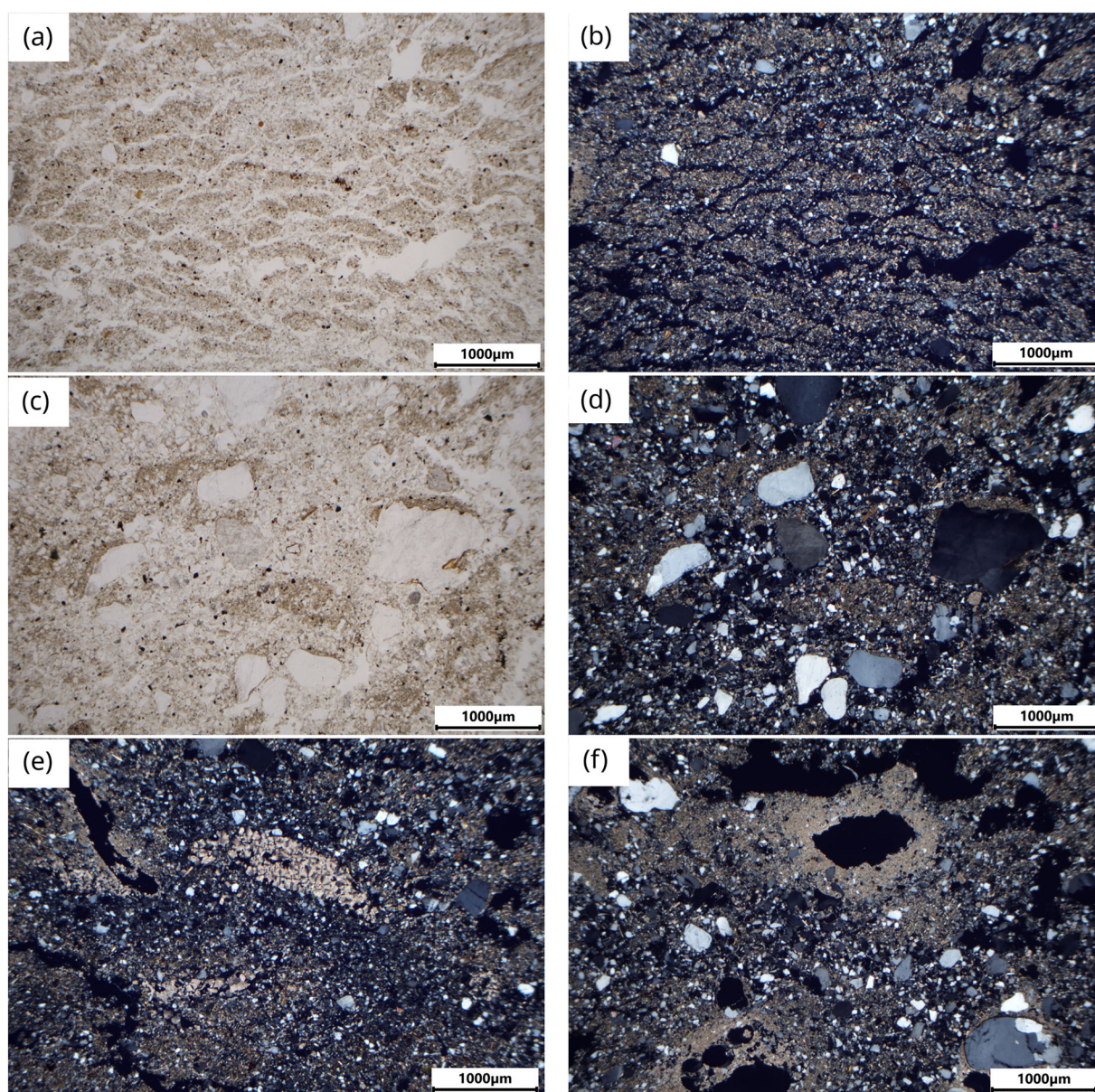


FIGURE 7 Images of thin sections MM2. (a + b) lenticular platy microstructure (ppl + xpl; MM2). (c + d) sparitic and micritic capping of larger grains (ppl + xpl; MM2). (e + f) secondary sparitic and micritic carbonates (xpl; MM2). The analysis of thin section MM3 shows a rather gradual transition over several millimeters for the macroscopically sharp boundary between the upper sandy loess from which carbonates have been leached and the lower sandy loess where secondary carbonates have accumulated (images not displayed). [Color figure can be viewed at wileyonlinelibrary.com]

4.4 | Section Rab2

At the base of Section Rab2 below a depth of about 180–200 cm (Figure 8), an accumulation of gravels can be found. The gravels display an advanced degree of physical weathering and are intertwined with the overlying silty-sandy material.

Between 50 cm and 180–200 cm below surface, the section is composed of a silty-sandy material with a GSD (Figure 8) (S1) that is very similar to the sandy loess in Section Rab1. While the upper part

of this sandy loess deposit has been pedogenetically altered in analogy to Section Rab1, the lower part (>150 cm) is composed of sandy loess that contains primary and secondary carbonates (CaO content = 9.5%, pH value = 7.5). These latter layers/horizons (Btb/E and CBwb) display a strong dip towards the right side of the exposed section. Furthermore, pedogenetic features similar to Section Rab1 can be observed, especially the formation of a Bt horizon with elevated clay contents (8.5%). In the horizon right below, banded clay features are visible, although not many and as well preserved as in

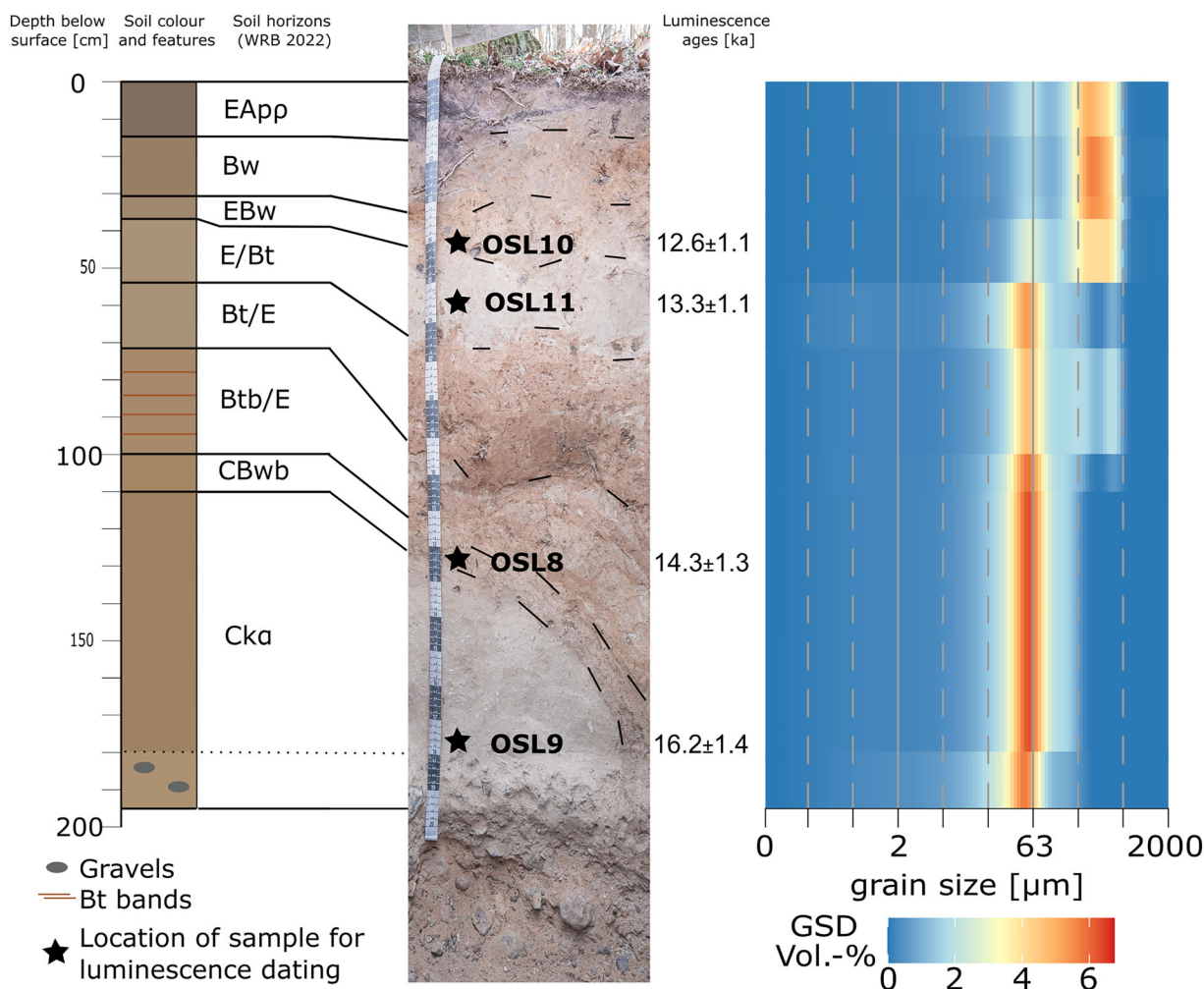


FIGURE 8 Section Rab2: image, sampling locations/depths, soil horizons (IUSS working group WRB 2022), luminescence ages and heat map of grain size distribution. [Color figure can be viewed at wileyonlinelibrary.com]

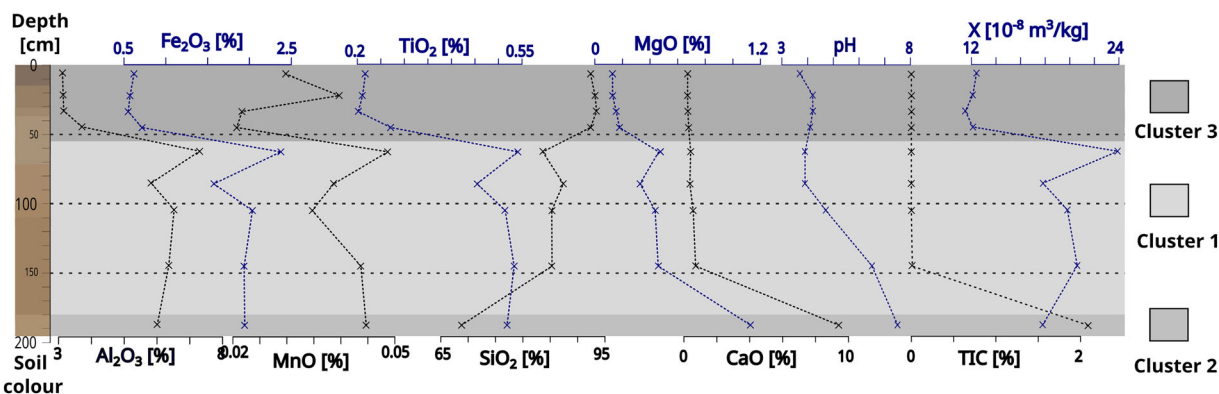


FIGURE 9 Geochemical data and clusters for Section Rab2. [Color figure can be viewed at wileyonlinelibrary.com]

Section Rab1. In contrast to Section Rab1, the upper unit of this section is assigned to Geochemical Cluster 3, whereas the underlying unit down to a depth of 1.5 m below surface is assigned to Geochemical Cluster 1 (Figure 9). The lowermost sample from the carbonatic sandy loess is assigned to Geochemical Cluster 2.

The uppermost unit of Section Rab2 is composed of sandy(–silty) material with a main mode in the medium sand fraction between 200 and 300 μm and a minor mode in the coarse silt fraction (Figure 8). The lower part of this unit (E/Bt, 37–54 cm) represents a transition zone between the upper and the lower unit. Within the upper 50 cm, pH values are comparatively low (3.7–4.2) and macroscopic signs of chemical weathering and podzolisation are visible.

The mean depositional age of the sandy loess (OSL8 and OSL9) was measured to be 15.3 ± 1.0 ka (Figure 8). These ages are in the range of the ages found in the upper part of Section Rab1 (OSL6 and OSL7). Two luminescence ages were derived from the uppermost unit, yielding a mean age of 13.0 ± 0.4 ka.

4.5 | Section Rab3

Macroscopically and with respect to pedogenesis, Section Rab3 (Figure 10) is broadly similar to Sections Rab1 and Rab2. The pedogenetically modified part of the sections reaches a depth of about

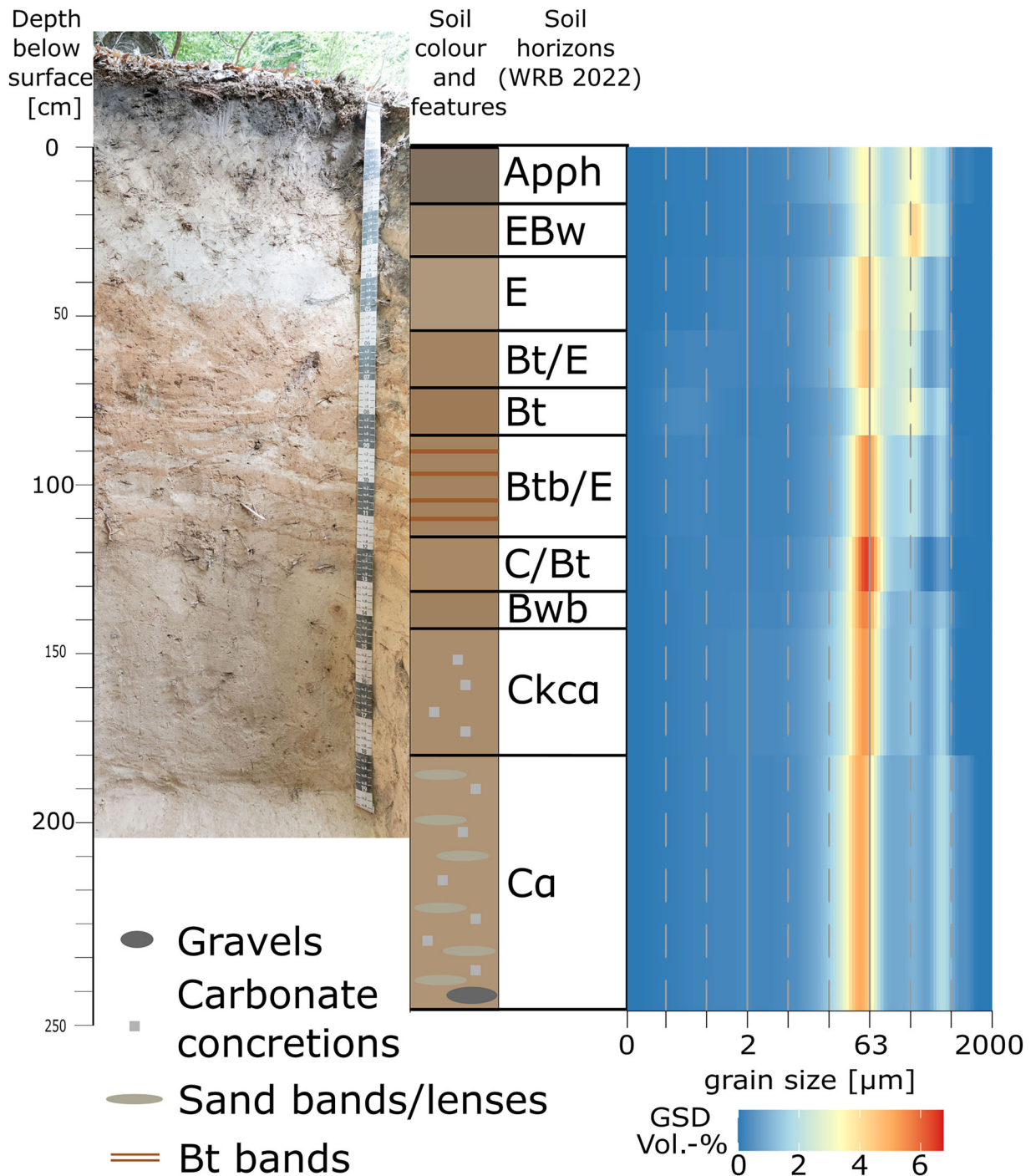


FIGURE 10 Section Rab3: image, sampling locations/depths, soil horizons [IUSS working group WRB 2022] and heat map of grain size distribution. [Color figure can be viewed at [wileyonlinelibrary.com](https://onlinelibrary.wiley.com)]

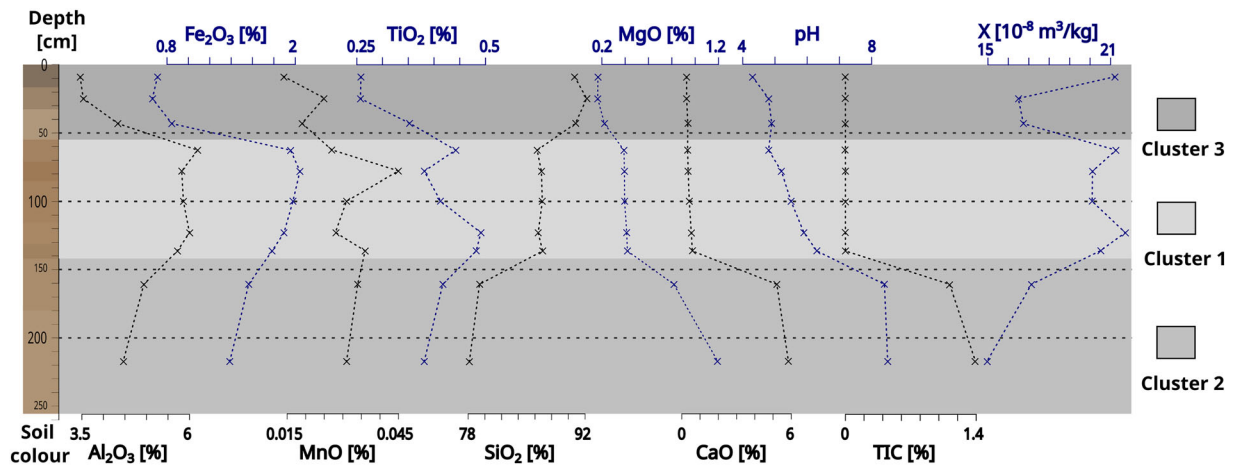


FIGURE 11 Geochemical data and clusters for Section Rab3. [Color figure can be viewed at wileyonlinelibrary.com]

1.4 m. At the base of the section (not shown in the photograph in Figure 10), single gravels were found.

In its lower unit (80 cm and below), this section displays a GSD similar to Sections Rab1 and Rab2, with a pronounced peak in the coarse silt (and fine sand) fraction (Figure 10) (S1). However, thin layers or lenses of sand are well developed in this section and clearly visible in the field as well as in the GSD indicated by a peak in the medium sand fraction that is more pronounced compared to Sections Rab1 and Rab2. In the upper unit of Section Rab3 (above 80 cm below surface), a third and dominant mode around 200 μm is clearly distinguishable (Figure 10).

Geochemically, the upper part of the section (down to 55 cm below surface), corresponds to Cluster 3 (Figure 11), in analogy to Section Rab2. This cluster is characterised by high contents of SiO_2 and low contents of most other oxides (S4) as well as low pH values. The middle part of the section (55–140 cm) corresponds to Cluster 1, characterised by high contents of Al_2O_3 , Fe_2O_3 and TiO_2 and elevated levels of χ compared to the other clusters. The lower part of the sections corresponds to Cluster 2, with high contents of CaO and MgO (carbonates) and high pH values, while the contents of SiO_2 are particularly low.

5 | DISCUSSION

5.1 | Genesis of soil–sediment sections

The geophysical and geochemical data from all three sediment sections studied here draw a clear picture regarding sedimentation processes and subsequent soil formation. From a sedimentological point of view, the sections are composed of three facies.

The oldest and lowermost facies, which form the lowermost part of Section Rab1, consist of glacio-fluvial sandy material deposited during the Saalian glaciation (MIS 6). This facies corresponds to geochemical cluster 3. In Section Rab1, no remains of an Eemian soil are present. Consequently, all deposits that may have accumulated before the loess deposition in late MIS 2 must have been eroded and therefore created this extensive chronostratigraphic hiatus.

A silty–sandy facies with a bi-modal GSD was deposited during the late last Pleniglacial (MIS 2, 19–14 ka). While this facies is dominated by a mode in the coarse silt fraction, there is a secondary mode in the medium sand fraction that is realised in the form of thin layers. It most likely originates from the surrounding glacio-fluvial sands and was relocated during times or events with elevated wind speeds or different wind directions compared to the silty material. This would also explain the varying sand content within the three sections. In the lower parts of all three sediment sections, this facies contains primary and partly secondary carbonates that have been leached from the upper parts of the sections, attesting to the primary carbonatic nature of this facies. Geochemically, it is differentiated into Clusters 1 and 2, mainly due to the difference in carbonate content. The GSD allows for the classification of this facies as loess (sand content < 20%) or sandy loess (>20%). In any case, GSD is only slightly coarser than the GSD reported by Krauß et al. (2016) for loess deposits from Hecklingen and Zilly in the main loess area further west (Figure 2), including the secondary mode in the medium sand fraction. Furthermore, these GSD are in line with results obtained by Dobers (2002) in his study of sandy loess deposits in the Central Fläming near Jüterbog, where sand contents were usually below 20% or even below 15%.

For other loess sections in Central Eastern Germany, similar loess deposition ages were reported (Kreutzer et al., 2014; Lauer et al., 2014; Meszner et al., 2013; Schmidt et al., 2021). Based on these findings and the underlying compositional similarity between the sandy loess from the Fläming ridge and the deposits from the main loess areas, we propose to incorporate the former into the loess deposits of Central Eastern Germany, despite their historical differentiation from the latter and the inconsistencies related to the somewhat arbitrary threshold of 20% of sand separating loess and sandy loess. In their study of loess deposits in the Rhône Valley, Bosq et al. (2018) applied a different threshold for the differentiation of loess and sandy loess. This is in line with the loess definition proposed by Koch and Neumeister (2005), who proposed a geomorphological term for the alternation between silty and sandy layers, *variagenese* (*Variagenese*). Although no luminescence dating results and detailed GSD data have been published from sandy loess deposits in Northern Germany, results reported by Gehrt (1994) and Vierhuff (1967) point in the same direction. They also confirm earlier geomorphological and

chronostratigraphic interpretations in our study area that stress the spatial and chronological connection between the sandy loess and cover sand deposits (Lembke et al., 1970).

The derived depositional ages for the sandy-silty facies during periglacial times (19–14 ka) could be attested by the obtained micromorphological results. The lenticular platy microstructure in combination with a (micritic) capping of larger grains are clear indicators for periglacial conditions in the form of the formation of ice lenses as well as cryoturbatic and solifluidal processes (Bertran & Texier, 1999; Scarciglia et al., 2003; Todisco & Bhiry, 2008; van Vliet-Lanoë & Fox, 2018). As these phenomena were detected at a depth of approximately 350 cm below surface well below the influence of current freezing, they clearly indicate cold (periglacial) conditions during the time of (re)deposition of the sandy loess deposits in the late MIS 2.

In Sections Rab2 and Rab3, a third facies could be detected: Cover sands of about 50–70-cm thickness, geochemically corresponding to Cluster 3, attesting to their source in the glacio-fluvial material dominating in the surrounding areas. The deposition/formation of these cover sands occurred around 13 ka during the late MIS 2, in analogy to the sand sheet phase (lithostratigraphy: Older Coversands II or Younger Coversands I) for deposits in the Netherlands (Kasse, 2002; Kasse & Aalbersberg, 2019). Hirsch et al. (2017) as well as Hilgers (2007) report late Pleistocene ages for sand deposits at the base of a dune near Glashütte within the Glogau-Baruther IMV. Based on dune morphology in this area, westerly (and southerly) paleo-wind directions are inferred (de Boer, 1995; Hirsch et al., 2017). For two other dune systems in central Brandenburg, Schlaak (2018) reports initial depositional ages during the Younger Dryas. Based on our geochronological data, it seems likely that the cover sands of the High Fläming pre-date the main phase of dune formation during the Older and Younger Dryas, which was also reported for dunes in Central Poland (Moska et al., 2023) and corresponds to the first cluster of (Late Glacial and Holocene) aeolian activity identified in a meta-study by Kappler et al. (2019) for north-eastern Germany.

Although error margins of the luminescence dating results presented here do not allow for a precise assignment to any specific stadial period during the late MIS 2, our results confirm the hypothesis of a Late Glacial (Weichselian) genesis of the Upper Layer (*Hauptlage*) (Hülle et al., 2009), to which the cover sands presented here most likely correspond (Altermann et al., 2008). Waroszewski et al. (2021) and Waroszewski et al. (2020) report ages between 14 and 11 ka for thin loess mantles (few decimeters) in south-western Poland, whose stratigraphic position corresponds to periglacial cover beds following Kleber & Terhorst (2013). However, more datings are needed to confirm this result, especially since luminescence dating of the Upper Layer has been a major challenge due to several methodological restraints (Kleber & Terhorst, 2013).

5.2 | Spatial distribution of sandy loess deposits

Generally, the modelled distribution pattern corresponds roughly to the extent of sandy loess published by Lehmkuhl et al. (2020). Our interpolation highlights the patchy distribution and the varying thickness (up to 200 cm) of the loess accumulations, which strikingly reflects the small-scale depositional and erosional processes that need to be considered when interpreting loess landscapes.

Periglacial dry valleys (Rummeln) are landforms typical of the study area. We observed a spatial correlation between the occurrence of these dry valleys and the main sandy loess distribution areas. This spatial correlation appears straightforward, as these special types of dry valleys are a characteristic geomorphic feature of loess landscapes associated with Holocene soil erosion (Lehmkuhl et al., 2016; Rommens et al., 2007). As it was shown, in some places there is no sandy loess inside the dry valleys, whereas the prediction sometimes indicates sandy loess deposits inside the dry valleys (Figure 4f). This is possibly related to the heterogeneous distribution of drilling points and the kriging model itself, which does not incorporate geomorphological parameters. Nonetheless, it is also possible that sandy loess material was eroded from the plateau areas and redeposited after a short transport distance on the valley bottoms as colluvial material.

Furthermore, the spatial distribution of sandy loess visible in the kriging prediction resembles the pattern that can be found across the entire Fläming ridge, that is, thick deposits are mainly located on the northern edge of the belt, whereas the deposits decrease in thickness towards the southern part of the ridge (Altermann & Fiedler, 1972b). However, on a finer spatial scale, the distribution pattern is rather complex. This likely results from two main reasons:

1. Methodology: The density of drill points in the area is too low for the desired resolution. The mean nearest neighbour distance (111 m) is close to the variogram range, thus predictions will deviate frequently considerably from the unknown truth at unsampled sites. Furthermore, it remains unknown how relocated sediments (colluvial, flood loam) with sandy loess textures were classified during the original drilling/mapping campaign. This may explain the existence of modelled sandy loess covers within the dry valleys, where relocation of sediments will surely have happened during the Holocene (and potentially already during the late Weichselian).
2. Furthermore, the paleo-relief has been reshaped since the time of sandy loess deposition by periglacial processes during the (late) Weichselian and by denudation and (soil) erosion during the Holocene. Long-lasting and intense land use has been proven for many loess areas in Central Europe. For a catchment of 10 km² in a loess landscape (Wetterau) near Frankfurt a.M. (Germany) which has been settled since Neolithic times, Houben (2012) calculated a mean denudation rate of 64 cm during the Holocene. While there is only little proof of Neolithic activity in the Fläming area so far (Cziesla, 2008; Eberhardt, 2007; Mischka & Wetzel, 2015), the sandy loess area has experienced intense agricultural land use based on the fertility of soils at least since medieval times (Liedtke & Marcinek, 2002). Therefore, features of the paleo-relief explaining loess deposition may now be missing or may have been morphologically transformed.

Consequently, the obtained results regarding (sandy) loess distribution in the Fläming area led to promising first interpretations. Based on an extended dataset (current survey of the whole Fläming ridge by the state geological survey) and modern methods for the calculation of the local or regional paleo-relief (Schmidt et al., 2018), a more detailed understanding of the original spatial distribution patterns in relation to the (paleo)relief is an important future task.

5.3 | Chronostratigraphy, source areas and paleoclimatic interpretation of (sandy) loess deposits in the Fläming ridge

As potential source areas for the sandy loess deposits on the Fläming ridge, Maudrei (1968) and Altermann and Fiedler (1972a) propose mainly northerly winds and corresponding source areas in the adjacent low-lying areas to the north and north-east (Glogau-Baruther IMV, till plains) (Figure 12). Their model helps to explain the gradual increase in (coarse) silt contents on the northern edge and the abrupt decrease at the southern edge of the (sandy) loess belt, which was confirmed by the model results of this study (Figure 4). Furthermore, the sandy loess deposits in the western part of the Fläming loess belt are considerably thicker, which cannot be satisfactorily explained in combination with dominating westerly winds which have been assumed and found (Prud'homme et al., 2022) to be the dominant winds during the LGM and Late Pleistocene in Central Europe in analogy to modern conditions. Given the elongated shape of the (sandy) loess belt in the Fläming area with its marked NW-SE extension, it appears most likely that repeated dust events caused by northerly and north-easterly winds resulted in the depositional pattern.

In a similar line of thought, Badura et al. (2013) proposed a regional model of fluvial transport of silty material originating from the Central European Highlands along the valley of the Great Odra River, which corresponds to the Wrocław-Magdeburg-Bremen IMV

in the study area (Figure 12). This is in analogy to the global model of loess originating from the large braided river systems proposed by Smalley et al. (2009). The Great Odra Valley (GOV) was originally formed as an IMV during the Saalian glaciation. Analogous to loess genesis models related to other Central European rivers like the Rhine or the Danube, these silty sediments would have been blown out of the episodically desiccated GOV (in MIS 4 and MIS 2) and would have eventually formed the Central European loess covers. This hypothesis has already been confirmed for loess deposits in south-western Poland; however, a significant contribution of the FIS was also detected, probably by erosion of older glacial and/or glacio-fluvial sediments and recycling of loess deposits (Waroszewski et al., 2021). With respect to the amounts of loess deposited in Eastern and Central Germany, only a large catchment area like the one assigned to the GOV would have supplied a sufficient amount of fine material in order for the extensive loess covers in Saxony, Saxony-Anhalt and Lower Saxony to be formed (Badura et al., 2013). Applying this model to the (sandy) loess deposits on the Fläming ridge, these would represent a minor loess area compared to the main loess areas to the south and west due to the limited amount of silty material in the source areas to the north (Figure 12). Since the (primary) sandy loess deposits of the Fläming area comprised a considerable amount of carbonates which are rare in the Glogau-Baruther IMV, the till plains and carbonatic glacio-limnic deposits to the north of the IMV must also have contributed significantly to the dust load and deposition. These deposits lie within the area that north-easterly winds

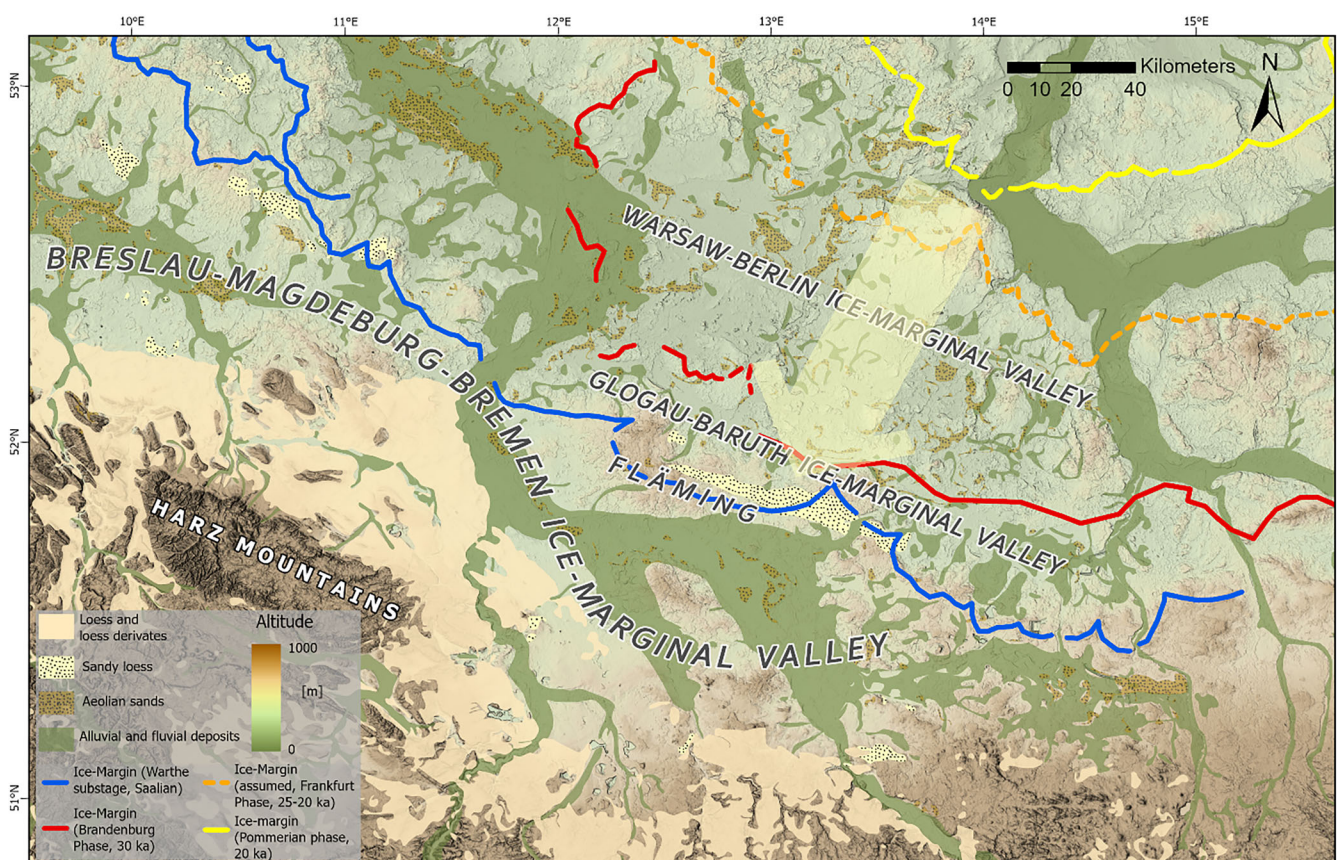


FIGURE 12 Location of potential source areas for main loess areas in Central Eastern Germany (MIS 4 and MIS 2) and for (sandy) loess in the Fläming area (MIS 2). The bold yellow arrow represents potential wind and dust trajectory during late MIS 2. The distribution of deposits mapped based on data published by (Lehmkuhl et al., 2021). Ice margins mapped based on data published by Lüthgens et al. (2020) and Liedtke (1981). Digital surface model (DSM) based on ESA (2022). [Color figure can be viewed at [wileyonlinelibrary.com](https://onlinelibrary.wiley.com)]

coming from the FIS would have crossed on their way towards the Fläming ridge (Figure 12).

Based on a comparison of trace elements between samples from different loess sections and of different ages (MIS 4 and MIS 2) in Saxony that displayed little variation between samples, Meszner et al. (2013) concluded that the source area of loess deposits from Saxony did not change during main loess deposition phases within the Weichselian period. However, in the same study, coarse components within the loess sections were found to have been transported mainly by north-westerly winds based on the heavy mineral composition and abundance. In a related study, Meszner et al. (2014) identify the nearby Elbe Valley to be the most likely dust source for the main loess deposits in Saxony. Furthermore, the uppermost loess (Unit IIa) of the Gleina section (Meszner et al., 2013) contains elevated contents of (fine) sand, which is interpreted as an indicator for increased wind speeds and resembles the sandy banded loess deposits of the Fläming area.

Current model results (Ludwig et al., 2016) indicate prevailing easterly winds in Central Europe during the LGM caused by a strong anticyclone over the FIS, which is in favour of the model proposed here. Like loess deposits in Western and Southern (Central) Europe (Lehmkuhl et al., 2016, 2021; Pötter et al., 2021, 2023), alluvial and fluvial deposits within the large (ice-marginal) valleys as well as till plains serve as the main source areas of loess deposits. On the regional scale, the Glogau-Baruther IMV and the till plains in the area of Brandenburg can be considered as the main source area of the loess deposits on the Fläming ridge. This hypothesis of a dominance of easterly winds was confirmed by results obtained by Schaffernicht et al. (2020), who identified the southern FIS margin to be the area with the highest dust (loess) emission (and deposition) rates. A shift to a dominance of westerly winds as indicated by parabolic dunes near the study area (Section 5.1) must have happened in close accordance with the ongoing downwasting of the FIS. It remains questionable why the loess distribution in the study area does not continue further to the south-east. This may be connected to open questions regarding the location and extent of the LGM ice-sheet advance in the area of the modern German–Polish border as discussed by Lüthgens et al. (2020) (Figure 6 therein).

6 | CONCLUSIONS/OUTLOOK

On the Fläming ridge, aeolian deposits of silty to sandy composition were formed during the late MIS 2 (19–13 ka). They most likely originate from the lower lying areas (till plains, IMVs) to the north and north-east of the Fläming and were transported by katabatic winds coming from the FIS. This adds an important aspect to the discussion raised by many other studies related to Late Pleistocene loess deposits in Central Europe, in which dominant westerly wind directions and respective transport paths are inferred. Based on its GSD and chronostratigraphy, the (banded) sandy loess deposits of the Fläming ridge closely resemble the (youngest) loess deposits of the adjacent main loess areas to the south and the west of the Fläming ridge.

These results shed new light on the influence of the oscillating FIS regarding wind directions and wind speeds in the paraglacial environment. Furthermore, they underline the importance of the spatial

configuration of till plains and glacio-fluvial deposits as source areas for wind-blown particles. In contrast to the adjacent loess areas, the distribution of sandy loess was found to be more patchy, probably related to the relatively short period of deposition, the pre-existing morphology of the terrain as well as post-depositional intense erosion processes and surface modifications.

AUTHOR CONTRIBUTIONS

Fabian Kirsten: Conceptualisation; investigation; supervision; writing—initial draft; writing—reviewing and editing. **Joris Starke:** Investigation; software. **Albrecht Bauriegel:** Conceptualisation; funding acquisition; investigation; resources. **Robert Müller:** Investigation; software; writing—initial draft. **Jens Jouaux:** Investigation; software. **Christopher Lüthgens:** Methodology; investigation; writing—initial draft. **Ralf Sinapius:** Investigation; resources. **Jacob Hardt:** Conceptualisation; writing—initial draft; writing—reviewing and editing.

ACKNOWLEDGEMENTS

We gratefully acknowledge Nadav Nir for help with sampling (thin sections) and Susann Heinrich (Leipzig) for the analysis of thin sections. We also thank Margot Böse (FU Berlin) for very helpful discussions and comments regarding the contents of this study. Thanks to Philipp Schulte (RWTH Aachen) for providing measurements for the cross-validation of GSD. We would also like to thank two anonymous reviewers and the editor for helpful and constructive comments on earlier versions of this manuscript. Open Access funding enabled and organized by Projekt DEAL.

DATA AVAILABILITY STATEMENT

All data related to this study can be found in the supplementary online information or will be made available upon request to the corresponding author.

ORCID

Fabian Kirsten  <https://orcid.org/0000-0002-4813-3713>

Joris Starke  <https://orcid.org/0009-0007-4832-9752>

Robert Müller  <https://orcid.org/0009-0004-4191-5511>

Jacob Hardt  <https://orcid.org/0000-0001-8485-2232>

REFERENCES

- Adamiec, G. & Aitken, M.J. (1998) Dose–rate conversion factors: update. *Ancient TL*, 16, 37–50.
- Aitchison, J. (1982) The statistical analysis of compositional data. *Journal of the Royal Statistical Society: Series B: Methodological*, 44, 139–177. [online] Available from: <https://www.jstor.org/stable/2345821> [Accessed 28th May 2023].
- Altermann, M. (1993) *Gliederung und Lithologie pleistozäner Lagen im Gebiet Sachsen-Anhalts*. In: Hugenroth, P. (Ed.) *Mitteilungen der deutschen bodenkundlichen Gesellschaft*, Band 72, Heft 2, pp. 819–824.
- Altermann, M. & Fiedler, H.-J. (1972a) Einige Ergebnisse von Untersuchungen an weichselzeitlichen äolischen Deckschichten in einem Teil des Altmoränengebietes der DDR (Sachsen-Anhalt). *Zpra'vy, Geografickeho ustavu CSAV*, IX, 1–25.
- Altermann M, Fiedler H.-J. 1972b. Einige Ergebnisse von Untersuchungen an Weichselzeitlichen äolischen Deckschichten in einem Teil des Altmoränengebietes der DDR (Sachsen-Anhalt). *Mitteilung aus dem VEB Geologische Forschung und Erkundung Halle (S) und aus dem Bereich Bodenkunde und Standortslehre der Sektion Forstwirtschaft*.
- Altermann, M. & Fiedler, H.-J. (1978) Die Kennzeichnung der Böden in den Sandlössgebieten außerhalb des Lößgürtels der DDR unter

- besonderer Berücksichtigung des Substrataufbaues. *Beiträge zur Geographie*, 29, 157–199.
- Altermann, M., Jäger, K.-D., Kopp, D., Kowalkowski, A., Kühn, D. & Schwanecke, W. (2008) Zur Kennzeichnung und Gliederung von periglazial bedingten Differenzierungen in der Pedosphäre. *Waldökologie, Landschaftsforschung und Naturschutz*, pp. 5–42.
- Auclair, M., Lamothe, M. & Huot, S. (2003) Measurement of anomalous fading for feldspar IRSL using SAR. *Radiation Measurements*, 37(4–5), 487–492. Available from: [https://doi.org/10.1016/S1350-4487\(03\)00018-0](https://doi.org/10.1016/S1350-4487(03)00018-0) [online] Available from: <https://www.sciencedirect.com/science/article/pii/S1350448703000180>
- Badura, J., Jary, Z. & Smalley, I. (2013) Sources of loess material for deposits in Poland and parts of Central Europe: the lost Big River. *Quaternary International*, 296, 15–22. Available from: <https://doi.org/10.1016/j.quaint.2012.06.019> [online] Available from: <https://www.sciencedirect.com/science/article/pii/S1040618212004399>
- Bertran, P., Liard, M., Sitzia, L. & Tissoux, H. (2016) A map of Pleistocene aeolian deposits in Western Europe, with special emphasis on France. *Journal of Quaternary Science*, 31(8), e2909. Available from: <https://doi.org/10.1002/jqs.2909>
- Bertran, P. & Texier, J.-P. (1999) Facies and microfacies of slope deposits. *Catena*, 35(2–4), 99–121. Available from: [https://doi.org/10.1016/S0341-8162\(98\)00096-4](https://doi.org/10.1016/S0341-8162(98)00096-4)
- Boden, A.G. (Ed). (2005) *Bodenkundliche Kartieranleitung: mit 41 Abbildungen, 103 Tabellen und 3L listen. 5., verbesserte und erweiterte Auflage. In: Kommission E. Schweizerbart'sche Verlagsbuchhandlung (Nägele und Obermiller). Stuttgart; Hannover: Bundesanst. für Geowiss. und Rohstoffe.*
- Bosq, M., Bertran, P., Degeai, J.-P., Kreutzer, S., Queffelec, A., Moine, O., et al. (2018) Last glacial aeolian landforms and deposits in the Rhône Valley (SE France): spatial distribution and grain-size characterization. *Geomorphology*, 318, 250–269. Available from: <https://doi.org/10.1016/j.geomorph.2018.06.010>
- Bosq, M., Kreutzer, S., Bertran, P., Lanos, P., Dufresne, P. & Schmidt, C. (2023) Last glacial loess in Europe: luminescence database and chronology of deposition. *Earth System Science Data*, 15(10), 4689–4711. Available from: <https://doi.org/10.5194/essd-15-4689-2023>
- Bøtter-Jensen, L., Andersen, C.E., Duller, G.A.T. & Murray, A.S. (2003) Developments in radiation, stimulation and observation facilities in luminescence measurements. *Radiation Measurements*, 37(4–5), 535–541. Available from: [https://doi.org/10.1016/S1350-4487\(03\)00020-9](https://doi.org/10.1016/S1350-4487(03)00020-9) [online] Available from: <https://www.sciencedirect.com/science/article/pii/S1350448703000209>
- Bøtter-Jensen, L., Bulur, E., Duller, G.A.T. & Murray, A.S. (2000) Advances in luminescence instrument systems. *Radiation Measurements*, 32(5–6), 523–528. Available from: [https://doi.org/10.1016/S1350-4487\(00\)00039-1](https://doi.org/10.1016/S1350-4487(00)00039-1) [online] Available from: <https://www.sciencedirect.com/science/article/pii/S1350448700000391>
- Bøtter-Jensen, L., Thomsen, K.J. & Jain, M. (2010) Review of optically stimulated luminescence (OSL) instrumental developments for retrospective dosimetry. In: *Proceedings of the 7th European Conference on Luminescent Detectors and Transformers of Ionizing Radiation (LUMDETR 2009)*, Vol. 45, pp. 253–257 <https://doi.org/10.1016/j.radmeas.2009.11.030> [online] Available from: <https://www.sciencedirect.com/science/article/pii/S1350448709003126>
- Bullard, J.E. (2013) Contemporary glacial inputs to the dust cycle. *Earth Surface Processes and Landforms*, 38(1), 71–89. Available from: <https://doi.org/10.1002/esp.3315>
- Bullock, P., Fedoroff, N. & Jongerius, A. (1985) *Handbook for soil thin section description*. Albrighton: Waine Research Publ.
- Buylaert, J.-P., Jain, M., Murray, A.S., Thomsen, K.J., Thiel, C. & Sohbati, R. (2012) A robust feldspar luminescence dating method for middle and late Pleistocene sediments. *Boreas*, 41(3), 435–451. Available from: <https://doi.org/10.1111/j.1502-3885.2012.00248.x> [online] Available from: <https://www.scopus.com/inward/record.uri?eid=2-s2.0-84862752963&doi=10.1111/j.1502-3885.2012.00248.x&partnerID=40&md5=b8f25534eb7c7e32c48162cf09fb909d>
- Buylaert, J.P., Murray, A.S., Thomsen, K.J. & Jain, M. (2009) Testing the potential of an elevated temperature IRSL signal from K-feldspar. *Radiation Measurements*, 44(5–6), 560–565. Available from: <https://doi.org/10.1016/j.radmeas.2009.02.007> [online] Available from: <https://www.sciencedirect.com/science/article/pii/S1350448709000316>
- Castillo, C. & Gómez, J.A. (2016) A century of gully erosion research: urgency, complexity and study approaches. *Earth-Science Reviews*, 160, 300–319. Available from: <https://doi.org/10.1016/j.earscirev.2016.07.009>
- Cepek, A.G. (1959) Ergebnisse neuerer Untersuchungen im Pleistozän Brandenburgs. *Ber. Geol. Ges. DDR*, 4, 233–234.
- Cunningham, A.C. & Wallinga, J. (2012) Realizing the potential of fluvial archives using robust OSL chronologies. *Quaternary Geochronology*, 12, 98–106. Available from: <https://doi.org/10.1016/j.quageo.2012.05.007> [online] Available from: <https://www.sciencedirect.com/science/article/pii/S1871101412001069>
- Cziesla, E. (2008) Zur bandkeramischen kultur zwischen Elbe und Oder. *Germania*, 86, 405–464.
- Dammer, B. (1941) Über Flottsande in der östlichen Mark Brandenburg. *Jb. Reichsst. Bodenforsch.*, 61, 186–197.
- de Boer, W.M. (1995) *Äolische Prozesse und Landschaftsformen im mittleren Baruther Urstromtal seit dem Hochglazial der Weichselkaltzeit*. Berlin: Fachbereich Geographie der Humboldt-Universität zu Berlin.
- Deutsches Institut für Normung. (2020). Particle size analysis—laser diffraction methods. DIN/ISO 13320:2020-01.
- Deutsches Institut für Normung. 2022. *Soil, treated biowaste and sludge—determination of pH DIN/ISO 10390:2022-08*. Beuth-Verlag.
- Diggle, P.J. & Ribeiro, P.J., Jr. (2007) *Model-based geostatistics*. New York, USA: Springer.
- Dobers, E.S. (2002) *Methoden der Standorterkundung als Grundlage der DGPS-gestützten Ackerbaus: eine Fallstudie aus dem Lössgebiet des Mittleren Fläming: dissertation*. Göttingen: Georg-August-Universität Göttingen.
- Dunn, J.C. (1974) Well-separated clusters and optimal fuzzy partitions. *Journal of Cybernetics*, 4(1), 95–104. Available from: <https://doi.org/10.1080/01969727408546059> (Accessed 28 May 2023).
- Eberhardt, G. (2007) Jungsteinzeitliche Funde vom Nuthe-Oberlauf bei Jüterbog, Lkr. Teltow-Fläming. Zur Neolithisierung einer brandenburgischen Kleinregion. *Forschungen zur Archäologie im Land Brandenburg*, 10, 9–110.
- Eissmann, L., Litt, T. & Wansa, S. (2020) Elsterian and Saalian deposits in their type area in central Germany. In: Ehlers, J., Kozarski, S., Gibbard, P.L. & Rose, J. (Eds.) *Glacial deposits in north-east Europe*. Boca Raton, FL: CRC Press, pp. 439–464. <https://doi.org/10.1201/9781003077695-55>
- ESA. (2022). *Copernicus DEM: EEA-10*. <https://doi.org/10.5270/ESA-c5d3d65>
- Fiedler, H.-J. & Altermann, M. (1964) Verbreitung, Entstehung und Eigenschaften von Sandlöß (Flottsand) im Norddeutschen Flachland und angrenzenden ebieten. *Geologie*, 13, 1199–1228.
- Galbraith, R.F., Roberts, R.G., Laslett, G.M., Yoshida, H. & Olley, J.M. (1999) Optical dating of single and multiple grains of quartz from Jinnium rock shelter, northern Australia: part I, experimental design and statistical models. *Archaeometry*, 41(2), 339–364. Available from: <https://doi.org/10.1111/j.1475-4754.1999.tb00987.x>
- Gehrt, E. (1994) *Die äolischen Sedimente im Bereich der nördlichen Lössgrenze zwischen Leine und Oker und deren Einflüsse auf die Bodenentwicklung*, [Dissertation]. Göttingen: Universität Göttingen.
- Gehrt, E. (2014) Nord- und mitteldeutsche Lössböden und Die Sandlössgebiete. In: Blume, H. (Ed.) *Handbuch der Bodenkunde*. Weinheim: Wiley-VCH, pp. 1–60.
- Geobasis-DE/LGB. (2020). *Digital terrain model of Brandenburg: dl-de/by-2-0* [online] Available from: <https://data.geobasis-bb.de/geobasis/daten/dgm/>
- GeoSN. 2021. *Digital terrain model of Saxony: dl-de/by-2-0* [online] Available from: <https://www.geodaten.sachsen.de/downloadbereich-digitale-hoehenmodelle-4851.htm>
- Haase, D., Fink, J., Haase, G., Ruske, R., Pécsi, M., Richter, H., et al. (2007) Loess in Europe—its spatial distribution based on a European loess map, scale 1:2,500,000. *Quaternary Science Reviews*, 26(9–10), 1301–1312. Available from: <https://doi.org/10.1016/j.quascirev.2007.02.003>

- Hardt, J. (2017) *Weichselian phases and ice dynamics of the Scandinavian Ice Sheet in Northeast Germany: A reassessment based on geochronological and geomorphological investigations in Brandenburg*. [Dissertation], Vol. 66. Berlin: Freie Universität Berlin, pp. 101–102.
- Hardt, J., Lüthgens, C., Hebenstreit, R. & Böse, M. (2016) Geochronological (OSL) and geomorphological investigations at the presumed Frankfurt ice marginal position in Northeast Germany. *Quaternary Science Reviews*, 154, 85–99. Available from: <https://doi.org/10.1016/j.quascirev.2016.10.015>
- Hartigan, J.A. & Wong, M.A. (1979) Algorithm AS 136: a K-means clustering algorithm. *Journal of the Royal Statistical Society: Series C: Applied Statistics*, 28, 100–108. Available from: <https://doi.org/10.2307/2346830> [online] Available from: <https://www.jstor.org/stable/2346830> [Accessed 24th November 2023].
- Hennig, C. (2007) Cluster-wise assessment of cluster stability. *Computational Statistics & Data Analysis*, 52(1), 258–271. Available from: <https://doi.org/10.1016/j.csda.2006.11.025> [online] Available from: <https://www.sciencedirect.com/science/article/pii/S0167947306004622> (Accessed 28 May 2023).
- Hilgers, A. (2007) *The chronology of Late Glacial and Holocene dune development in the northern Central European lowland reconstructed by optically stimulated luminescence (OSL) dating*. [Dissertation]. Köln: Universität zu Köln.
- Hirsch, F., Spröte, R., Fischer, T., Forman, S.L., Raab, T., Bens, O., et al. (2017) Late Quaternary aeolian dynamics, pedostratigraphy and soil formation in the North European Lowlands—new findings from the Baruther ice-marginal valley. *Die Erde*, 148(1), 58–73. Gesellschaft für Erdkunde.
- Houben, P. (2012) Sediment budget for five millennia of tillage in the Rockenberg catchment (Wetterau loess basin, Germany). *Quaternary Science Reviews*, 52, 12–23. Available from: <https://doi.org/10.1016/j.quascirev.2012.07.011>
- Hülle, D., Hilgers, A., Kühn, P. & Radtke, U. (2009) The potential of optically stimulated luminescence for dating periglacial slope deposits—a case study from the Taunus area, Germany. *Geomorphology*, 109(1–2), 66–78. Available from: <https://doi.org/10.1016/j.geomorph.2008.08.021>
- Huntley, D.J. & Baril, M.R. (1997) The K content of the K-feldspars being measured in optical dating or in thermoluminescence dating. *Ancient TL*, 15, 11–14.
- IUSS Working Group WRB. (2022) *World reference base for soil resources 2022: international soil classification system for naming soils and creating legends for soil maps*, 4th edition. Vienna, Austria: International Union of Soil Sciences.
- Kappler, C., Kaiser, K., Küster, M., Nicolay, A., Fülling, A., Bens, O., et al. (2019) Late Pleistocene and Holocene terrestrial geomorphodynamics and soil formation in northeastern Germany: a review of geochronological data. *Physical Geography*, 40(5), 405–432. Available from: <https://doi.org/10.1080/02723646.2019.1573621>
- Kasse, C. (2002) Sandy aeolian deposits and environments and their relation to climate during the Last Glacial Maximum and Lateglacial in northwest and central Europe. *Progress in Physical Geography: Earth and Environment*, 26(4), 507–532. Available from: <https://doi.org/10.1191/0309133302pp350ra>
- Kasse, C. & Aalbersberg, G. (2019) A complete late Weichselian and Holocene record of aeolian coversands, drift sands and soils forced by climate change and human impact, Ossendrecht, the Netherlands. *Netherlands Journal of Geosciences*, 98, e4. Available from: <https://doi.org/10.1017/njg.2019.3>
- Keilhack, K. (1906) *Geologische Spezialkarte von Preussen und den Thüringischen Staaten*. Kleipzig: Königlich Preussische Geologische Landesanstalt und Bergakademie.
- Kleber, A. & Terhorst, B. (2013) *Mid-latitude slope deposits (cover beds)*, 1st edition. Amsterdam: Elsevier. [online] Available from: <https://ebookcentral.proquest.com/lib/kxp/detail.action?docID=1170130>
- Klosa, D. (1994) Eine rechnergestützte methode zur bestimmung des gesamtcarbonatgehaltes in sedimenten und böden. *Zeitschrift für Angewandte Geologie*, 40, 18–21.
- Koch, R. & Neumeister, H. (2005) Zur klassifikation von Lönach genetischen kriterien. *Zeitschrift für Geomorphologie*, 49, 183–203. [online] Available from: <http://www.schweizerbart.de/papers/zfg/detail/49/64939/>
- Zur Klassifikation von Lösssedimenten nach genetischen Kriterien
Königlich Preussische Geologische Landesanstalt. (1908) *Geschäftsanweisung für die geologisch-agronomische Aufnahme im norddeutschen Flachlande*. Berlin.
- Krauß, L., Zens, J., Zeeden, C., Schulte, P., Eckmeier, E. & Lehmkuhl, F. (2016) A multi-proxy analysis of two loess-Paleosol sequences in the northern Harz foreland, Germany. *Palaeogeography, Palaeoclimatology, Palaeoecology*, 461, 401–417. Available from: <https://doi.org/10.1016/j.palaeo.2016.09.001>
- Krbetschek, M.R., Götze, J., Dietrich, A. & Trautmann, T. (1997) Spectral information from minerals relevant for luminescence dating. *Radiation Measurements*, 27(5–6), 695–748. Available from: [https://doi.org/10.1016/S1350-4487\(97\)00223-0](https://doi.org/10.1016/S1350-4487(97)00223-0) [online] Available from: <https://www.sciencedirect.com/science/article/pii/S1350448797002230>
- Kreutzer, S., Lauer, T., Meszner, S., Krbetschek, M., Faust, D. & Fuchs, M. (2014) Chronology of the quaternary profile Zeuchfeld in Saxony-Anhalt/Germany—a preliminary luminescence dating study. *Zeitschrift für Geomorphologie, Supplementary Issues*, 58(1), 5–26. Available from: <https://doi.org/10.1127/0372-8854/2012/S-00112>
- Kreutzer, S., Schmidt, C., Fuchs, M.C., Dietze, M., Fischer, M. & Fuchs, M. (2012) Introducing an R package for luminescence dating analysis. *Ancient TL*, 30, 1–8. [online] Available from: <https://hal.science/hal-01846159>
- Krige, D.G. (1951) A statistical approach to some basic mine valuation problems on the Witwatersrand. *Journal of the Southern African Institute of Mining and Metallurgy*, 52, 119–139. [online] Available from: https://journals.co.za/content/saimm/52/6/AJA0038223X_4792 (Accessed 27 May 2019).
- Kühn, P., Billwitz, K., Bauriegel, A., Kühn, D. & Eckelmann, W. (2006) Distribution and genesis of Fahlerden (Albeluvisols) in Germany. *Journal of Plant Nutrition and Soil Science*, 169(3), 420–433. Available from: <https://doi.org/10.1002/jpln.200521963>
- Kulig G. (2005). *Erstellung einer Auswertesoftware zur Altersbestimmung mittels Lumineszenzverfahren unter spezieller Berücksichtigung des Einflusses radioaktiver Ungleichgewichte in der 238U-Zerfallsreihe*. 35 p. B.Sc. thesis, Freiberg (Technische Universität Bergakademie Freiberg).
- Lauer, T., von Suchodoletz, H., Vollmann, H., Meszner, S., Frechen, M., Tinapp, C., et al. (2014) Landscape aridification in Central Germany during the late Weichselian Pleniglacial—results from the Zauschwitz loess site in western Saxony. *Zeitschrift für Geomorphologie, Supplementary Issues*, 58(1), 27–50. Available from: <https://doi.org/10.1127/0372-8854/2013/S-00163>
- Lehmkuhl, F., Nett, J.J., Pötter, S., Schulte, P., Sprafke, T., Jary, Z., et al. (2021) Loess landscapes of Europe—mapping, geomorphology, and zonal differentiation. *Earth-Science Reviews*, 215, 103496. Available from: <https://doi.org/10.1016/j.earscirev.2020.103496>
- Lehmkuhl, F., Pötter, S., Pauligk, A. & Böskén, J. (2018) Loess and other quaternary sediments in Germany. *Journal of Maps*, 14(2), 330–340. Available from: <https://doi.org/10.1080/17445647.2018.1473817>
- Lehmkuhl, F., Zens, J., Krauß, L., Schulte, P. & Kels, H. (2016) Loess-paleosol sequences at the northern European loess belt in Germany: distribution, geomorphology and stratigraphy. *Quaternary Science Reviews*, 153, 11–30. Available from: <https://doi.org/10.1016/j.quascirev.2016.10.008>
- Lehmkuhl F et al. 2020. *Geodata of European loess, sandy loess and aeolian sand*. <https://doi.org/10.5880/SFB806.56>
- Lembke, H., Altermann, M., Markuse, G. & Nitz, B. (1970) Die periglaziale Fazies im Alt- und Jungmoränengebiet nördlich des LAößgürtels. In: Richter, H., Haase, G., Lieberoth, I. & Ruske, R. (Eds.) *Periglazial - Löß - Paläolithikum im Jungpleistozän der DDR*. VEB Herrmann Haack, Geographisch-Kartographische Anstalt Gotha/Lei, pp. 213–279.
- Li, Y., Shi, W., Aydin, A., Beroya-Eitner, M.A. & Gao, G. (2020) Loess genesis and worldwide distribution. *Earth-Science Reviews*, 201, 102947. Available from: <https://doi.org/10.1016/j.earscirev.2019.102947>

- Liedtke, H. (1961) Geologischer Aufbau und geomorphologische Gestaltung im Fläming. In: Institut für Landeskunde. (Ed.) *Bericht zur deutschen Landeskunde* 26. Bad Godesberg: Bundesanstalt für Landeskunde und Raumforschung, pp. 45–81.
- Liedtke, H. (1981) Die Nordischen Vereisungen in Mitteleuropa. In: *Zentralausschuß für Dt.*, 2., erw. edition. Trier: Landeskunde.
- Liedtke, H. & Marcinek, J. (Eds.) (2002) 8.5.2 Stader Geest und südlicher Landrücken: Lüneburger Heide, Altmark, Fläming und Lausitzer Grenzwall. In: *Physische Geographie Deutschlands*. Gotha; Stuttgart: Klett-Perthes, pp. 440–446.
- Lippstreu, L., Hermsdorf, N., Sonntag, A. & Strahl, J. (2015) Quartär: Pleistozän. In: Stackebrandt, W. & Franke, D. (Eds.) *Geologie von Brandenburg*. Stuttgart: Schweizerbart, pp. 333–419.
- Ludwig, P., Schaffernicht, E.J., Shao, Y. & Pinto, J.G. (2016) Regional atmospheric circulation over Europe during the Last Glacial Maximum and its links to precipitation. *Journal of Geophysical Research-Atmospheres*, 121(5), 2130–2145. Available from: <https://doi.org/10.1002/2015JD024444>
- Lüthgens, C. & Böse, M. (2011) Chronology of Weichselian main ice marginal positions in north-eastern Germany. *E&G Quaternary Science Journal*, 60(2/3), 236–247. Available from: <https://doi.org/10.3285/eg.60.2-3.02>
- Lüthgens, C., Böse, M. & Krbetschek, M. (2010) On the age of the young morainic morphology in the area ascribed to the maximum extent of the Weichselian glaciation in north-eastern Germany. *Quaternary International*, 222(1–2), 72–79. Available from: <https://doi.org/10.1016/j.quaint.2009.06.028>
- Lüthgens, C., Hardt, J. & Böse, M. (2020) Proposing a new conceptual model for the reconstruction of ice dynamics in the SW sector of the Scandinavian Ice Sheet (SIS) based on the reinterpretation of published data and new evidence from optically stimulated luminescence (OSL) dating. *E&G Quaternary Science Journal*, 69(2), 201–223. Available from: <https://doi.org/10.5194/egqsj-69-201-2020>
- Lüthgens, C., Neuherber, S., Grupe, S., Payer, T., Peresson, M. & Fiebig, M. (2017) Geochronological investigations using a combination of luminescence and cosmogenic nuclide burial dating of drill cores from the Vienna Basin. *Zeitschrift der Deutschen Gesellschaft für Geowissenschaften*, 168(1), 115–140. Available from: <https://doi.org/10.1127/zdgg/2017/0081>
- Matheron, G. (1963) Principles of geostatistics. *Economic Geology*, 58(8), 1246–1266. Available from: <https://doi.org/10.2113/gsecongeo.58.8.1246> [online] Available from: <http://pubs.geoscienceworld.org/economicgeology/article/58/8/1246/17275/Principles-of-geostatistics> (Accessed 27 May 2019).
- Matheron, G. (1965) *Les variables régionalisées et leur estimation: une application de la théorie des fonctions aléatoires aux sciences de la nature*. Masson et CIE: Paris, France.
- Maudrei, F. (1968) *Geomorphologische, stratigraphische und paläogeographische Untersuchungen im Pleistozän des Niederen Fläming*, {Dissertation}. Berlin: Humboldt-Universität zu Berlin.
- Mejdahl V. (1979) Thermoluminescence dating: beta-dose attenuation in quartz grains. *Archaeometry*, 21(1), 61–72. Available from: <https://doi.org/10.1111/j.1475-4754.1979.tb00241.x>
- Meszner, S., Kreutzer, S., Fuchs, M. & Faust, D. (2013) Late Pleistocene landscape dynamics in Saxony, Germany: paleoenvironmental reconstruction using loess-paleosol sequences. *Quaternary International*, 296, 94–107. Available from: <https://doi.org/10.1016/j.quaint.2012.12.040>
- Meszner, S., Kreutzer, S., Fuchs, M. & Faust, D. (2014) Identifying depositional and pedogenetic controls of Late Pleistocene loess-paleosol sequences (Saxony, Germany) by combined grain size and microscopic analyses. *Zeitschrift für Geomorphologie, Supplementary Issues*, 58(3), 63–90. Available from: <https://doi.org/10.1127/O372-8854/2014/S-00169>
- Mischka, C. & Wetzell, R. (2015) Die ersten Bauern im Fläming. Geomagnetische Prospektion von Linearbandkeramischen Siedlungen bei Jüterbog, Lkr. Tektow-Fläming. *Archäologie in Berlin Und Brandenburg*, 2013, 48–52.
- Moska, P., Sokołowski, R.J., Zieliński, P., Jary, Z., Raczek, J., Mroczek, P., et al. (2023) An impact of short-term climate oscillations in the Late Pleniglacial and Lateglacial Interstadial on sedimentary processes and the pedogenic record in Central Poland. *Annals of the American Association of Geographers*, 113(1), 46–70. Available from: <https://doi.org/10.1080/24694452.2022.2094325>
- Muhs, D.R. (2014) Origins and Properties of Quaternary Loess Deposits. In: *Reference module in Earth systems and environmental sciences*. Elsevier.
- Nägler, K. (1926) Geologie und Biologie des Fläming. In: Nägler, K. & Kuhlmeier, W. (Eds.) *Durch den Hohen Fläming bei Belzig*. Neudamm: Neumann, pp. 5–36.
- Nebe, W., Altermann, M. & Fiedler, H.-J. (1962) Bemerkungen zum Geschiebedecksand. *Jb. Staatl. Mus. Mineral. Geol. Dresden*, pp. 147–155.
- Neumeister, H. (1965) Probleme der nördlichen Lößgrenze. *Leipziger Geografische Beiträge*, 137–143.
- Obst, T. & Kainz, W. (2020) In: Geologie, A.G. (Ed.) *Geologische Kartieranleitung, Sandstreifenlöss*. [online] Available from: <https://www.geokartieranleitung.de/Fachliche-Grundlagen/Genese-und-Geogenese/Geogenetische-Definition/Lockergesteine/entry/d2d470f3-ede4-4b13-aa12-8d317a5df304/mid/3427>
- Özer, M., Orhan, M. & Isik, N.S. (2010) Effect of particle optical properties on size distribution of soils obtained by laser diffraction. *Environmental and Engineering Geoscience*, 16(2), 163–173. Available from: <https://doi.org/10.2113/gsegeosci.16.2.163>
- Papritz A. 2021. *Georob: robust geostatistical analysis of spatial data. R package version 0.3–14* [online] Available from: <https://CRAN.R-project.org/package=georob>
- Patterson, H.D. & Thompson, R. (1971) Recovery of inter-block information when block sizes are unequal. *Biometrika*, 58(3), 545–554. Available from: <https://doi.org/10.2307/2334389> [online] Available from: <https://www.jstor.org/stable/2334389> (Accessed 14 October 2019).
- Pinto, J.G. & Ludwig, P. (2020) Extratropical cyclones over the North Atlantic and western Europe during the Last Glacial Maximum and implications for proxy interpretation. *Climate of the Past*, 16(2), 611–626. Available from: <https://doi.org/10.5194/cp-16-611-2020>
- Pötter, S., Seeger, K., Richter, C., Brill, D., Knaak, M., Lehmkuhl, F., et al. (2023) Pleniglacial dynamics in an oceanic central European loess landscape. *E&G Quaternary Science Journal*, 72(1), 77–94. Available from: <https://doi.org/10.5194/egqsj-72-77-2023>
- Pötter, S., Veres, D., Baykal, Y., Nett, J.J., Schulte, P., Hambach, U., et al. (2021) Disentangling sedimentary pathways for the pleniglacial Lower Danube loess based on geochemical signatures. *Frontiers in Earth Science*, 9. Available from: <https://doi.org/10.3389/feart.2021.600010>
- Prescott, J.R. & Hutton, J.T. (1994) Cosmic ray contributions to dose rates for luminescence and ESR dating: large depths and long-term time variations. *Radiation Measurements*, 23(2–3), 497–500. Available from: [https://doi.org/10.1016/1350-4487\(94\)90086-8](https://doi.org/10.1016/1350-4487(94)90086-8) [online] Available from: <https://www.sciencedirect.com/science/article/pii/S1350448794900868>
- Prescott JR, Stephan LG. 1982. The contribution of cosmic radiation to the environmental dose for thermoluminescence dating. Latitude, altitude and depth dependences [online] Available from: <https://api.semanticscholar.org/CorpusID:60041175>
- Prud'homme, C., Fischer, P., Jöris, O., Gromov, S., Vinnepand, M., Hatté, C., et al. (2022) Millennial-timescale quantitative estimates of climate dynamics in central Europe from earthworm calcite granules in loess deposits. *Communications Earth & Environment*, 3(1), 267. Available from: <https://doi.org/10.1038/s43247-022-00595-3>
- R Core Team. (2023) *R: a language and environment for statistical computing*. Vienna, Austria: R Foundation for Statistical Computing [online] Available from: <https://www.R-project.org/>
- Rades, E.F., Fiebig, M. & Lüthgens, C. (2018) Luminescence dating of the rissian type section in southern Germany as a base for correlation. *Quaternary International*, 478, 38–50. Available from: <https://doi.org/10.1016/j.quaint.2016.07.055> [online] Available from: <https://www.sciencedirect.com/science/article/pii/S1040618216302348>
- Reinecke, V. (2006) *Untersuchungen zur mittel- und jungpleistozänen Reliefentwicklung und Morphodynamik im nördlichen Harzvorland*, {Dissertation}. RWTH: Aachen.

- Rommens, T., Verstraeten, G., Peeters, I., Poesen, J., Govers, G., van Rompaey, A., et al. (2007) Reconstruction of late-Holocene slope and dry valley sediment dynamics in a Belgian loess environment. *The Holocene*, 17(6), 777–788. Available from: <https://doi.org/10.1177/0959683607080519>
- Rousseeuw, P.J. (1987) Silhouettes: a graphical aid to the interpretation and validation of cluster analysis. *Journal of Computational and Applied Mathematics*, 20, 53–65. Available from: [https://doi.org/10.1016/0377-0427\(87\)90125-7](https://doi.org/10.1016/0377-0427(87)90125-7) [online] Available from: <https://www.sciencedirect.com/science/article/pii/S0377042787901257> [Accessed 28th May 2023].
- Scarciglia, F., Terribile, F. & Colombo, C. (2003) Micromorphological evidence of paleoenvironmental changes in northern Cilento (South Italy) during the Late Quaternary. *Catena*, 54(3), 515–536. Available from: [https://doi.org/10.1016/S0341-8162\(03\)00124-3](https://doi.org/10.1016/S0341-8162(03)00124-3)
- Schaffernicht, E.J., Ludwig, P. & Shao, Y. (2020) Linkage between dust cycle and loess of the Last Glacial Maximum in Europe. *Atmospheric Chemistry and Physics*, 20(8), 4969–4986. Available from: <https://doi.org/10.5194/acp-20-4969-2020>
- Schlaak, N. (2018) Neue Untersuchungen an ünen in Brandenburg. *Brandenbur. Geowiss. Beitr.*, 25, 77–82.
- Schlather, M., Malinowski, A., Menck, P.J., Oesting, M. & Storkorb, K. (2015) Analysis, simulation and prediction of multivariate random fields with package RandomFields. *Journal of Statistical Software*, 63(8), 1–25. [online] Available from: <https://www.jstatsoft.org/v63/i08/>. Available from: <https://doi.org/10.18637/jss.v063.i08>
- Schlather, M., et al. (2022) RandomFields: simulation and analysis of random fields. *R Package Version 3.3.14* [online] Available from: Available from: <https://cran.r-project.org/package=RandomFields>
- Schmidt, J., Werther, L. & Zielhofer, C. (2018) Shaping pre-modern digital terrain models: the former topography at Charlemagne's canal construction site. *PLoS ONE*, 13(7), e0200167. Available from: <https://doi.org/10.1371/journal.pone.0200167>
- Schmidt, C., Zeeden, C., Krauß, L., Lehmkühl, F. & Zöller, L. (2021) A chronological and palaeoenvironmental re-evaluation of two loess-palaeosol records in the northern Harz foreland, Germany, based on innovative modelling tools. *Boreas*, 50(3), 746–763. Available from: <https://doi.org/10.1111/bor.12510>
- Schulte, P. & Lehmkühl, F. (2018) The difference of two laser diffraction patterns as an indicator for post-depositional grain size reduction in loess-palaeosol sequences. *Palaeogeography, Palaeoclimatology, Palaeoecology*, 509, 126–136. Available from: <https://doi.org/10.1016/j.palaeo.2017.02.022>
- Siebertz, H. (1988) Die Beziehung der äolischen Decksedimente in Nordwestdeutschland zur nördlichen Lösungsgrenze. *E&G Quaternary Science Journal*, 38(1), 106–114. Available from: <https://doi.org/10.3285/eg.38.1.10>
- Smalley, I., O'Hara-Dhand, K., Wint, J., Machalet, B., Jary, Z. & Jefferson, I. (2009) Rivers and loess: the significance of long river transportation in the complex event-sequence approach to loess deposit formation. *Quaternary International*, 198(1–2), 7–18. Available from: <https://doi.org/10.1016/j.quaint.2008.06.009>
- Sprafke, T. & Obrecht, I. (2016) Loess: rock, sediment or soil—what is missing for its definition? *Quaternary International*, 399, 198–207. Available from: <https://doi.org/10.1016/j.quaint.2015.03.033>
- Stoops, G. (2003) *Guidelines for analysis and description of soil and regolith thin sections*. Madison: Soil Science Soc. of America.
- Strauss, T. & von Maltitz, M.J. (2017) Generalising Ward's method for use with Manhattan distances. *PLoS ONE*, 12(1), e0168288. Available from: <https://doi.org/10.1371/journal.pone.0168288> [Accessed 28th May 2023].
- Todisco, D. & Bhiry, N. (2008) Micromorphology of periglacial sediments from the Tayara site, Qikirtaq Island, Nunavik (Canada). *Catena*, 76(1), 1–21. Available from: <https://doi.org/10.1016/j.catena.2008.08.002>
- Újvári, G., Kok, J.F., Varga, G. & Kovács, J. (2016) The physics of wind-blown loess: implications for grain size proxy interpretations in Quaternary paleoclimate studies. *Earth-Science Reviews*, 154, 247–278. Available from: <https://doi.org/10.1016/j.earscirev.2016.01.006>
- [online] Available from: <https://www.sciencedirect.com/science/article/pii/S001282521630006X>
- Vierhuff, H. (1967) Untersuchungen zur Stratigraphie und Genese der Sandlössvorkommen in Niedersachsen. *Mitteilungen aus dem Geologischen Institut der Technischen Hochschule Hannover*, 5, 1–99.
- Vinneband, M., Fischer, P., Hambach, U., Jöris, O., Craig, C.A., Zeeden, C., et al. (2023) What do dust sinks tell us about their sources and past environmental dynamics? A case study for oxygen isotope stages 3–2 in the Middle Rhine Valley, Germany. *E&G Quaternary Science Journal*, 72(2), 163–184. Available from: <https://doi.org/10.5194/egqsj-72-163-2023>
- van Vliet-Lanoë, B. & Fox, C.A. (2018) Frost Action. In: Stoops, G., Marcelino, V. & Mees, F. (Eds.) *Interpretation of micromorphological features of soils and regoliths Elsevier; EBSCO Industries Inc.* Amsterdam, Netherlands; Oxford, United Kingdom; Cambridge, United States; Ipswich, Massachusetts, pp. 81–108. Elsevier.
- Von Linstow, O. (1902) Ueber jungglaciale Feinsande des Fläming. *Jahrbuch der Preussischen Geologischen Landesanstalt*, 23, 278–295.
- Wald, A. (1943) Tests of statistical hypotheses concerning several parameters when the number of observations is large. *Transactions of the American Mathematical Society*, 54(3), 426–482. Available from: <https://doi.org/10.1090/S0002-9947-1943-0012401-3> [online] Available from: <http://www.ams.org/jourcgi/jour-getitem?pii=S0002-9947-1943-0012401-3> [Accessed 20th August 2019].
- Waroszewski, J., Pietranik, A., Sprafke, T., Kabała, C., Frechen, M., Jary, Z., et al. (2021) Provenance and paleoenvironmental context of the Late Pleistocene thin aeolian silt mantles in southwestern Poland—a widespread parent material for soils. *Catena*, 204, 105377. Available from: <https://doi.org/10.1016/j.catena.2021.105377>
- Waroszewski, J., Sprafke, T., Kabała, C., Musztyfaga, E., Kot, A., Tsukamoto, S., et al. (2020) Chronostratigraphy of silt-dominated Pleistocene periglacial slope deposits on Mt. Ślęza (SW, Poland): Palaeoenvironmental and pedogenic significance. *Catena*, 190, 104549. Available from: <https://doi.org/10.1016/j.catena.2020.104549>
- Webster, R. & Oliver, M.A. (2007) *Geostatistics for environmental scientists*, 2nd edition. Wiley: Chichester, UK.
- Wintle, A.G. & Murray, A.S. (2006) A review of quartz optically stimulated luminescence characteristics and their relevance in single-aliquot regeneration dating protocols. *Radiation Measurements*, 41(4), 369–391. Available from: <https://doi.org/10.1016/j.radmeas.2005.11.001> [online] Available from: <https://www.sciencedirect.com/science/article/pii/S1350448705003227>
- Zeeberg, J. (1998) The European sand belt in eastern Europe—and comparison of Late Glacial dune orientation with GCM simulation results. *Boreas*, 27(2), 127–139. Available from: <https://doi.org/10.1111/j.1502-3885.1998.tb00873.x>
- Zeileis, A. & Hothorn, T. (2002) Diagnostic checking in regression relationships. *R News*, 2, 7–10. [online] Available from: <https://CRAN.R-project.org/doc/Rnews/>
- Zoeller, L. (2010) New approaches to European loess: a stratigraphic and methodical review of the past decade. *Central European Journal of Geosciences*, 2(1), 19–31. Available from: <https://doi.org/10.2478/v10085-009-0047-y>

SUPPORTING INFORMATION

Additional supporting information can be found online in the Supporting Information section at the end of this article.

How to cite this article: Kirsten, F., Starke, J., Bauriegel, A., Müller, R., Jouaux, J., Lüthgens, C. et al. (2024) Age, composition and spatial distribution of sandy loess in north-eastern Germany (Fläming, Brandenburg). *Earth Surface Processes and Landforms*, 49(11), 3261–3282. Available from: <https://doi.org/10.1002/esp.5885>